

PARTICLE INTEGRITY, SAMPLING, AND APPLICATION OF A DNA-TAGGED TRACER
FOR AEROSOL TRANSPORT STUDIES

By

Cynthia Jeanne Kaeser

A DISSERTATION

Submitted to
Michigan State University
in partial fulfillment of the requirements
for the degree of

Chemistry – Doctor of Philosophy

2017

ABSTRACT

PARTICLE INTEGRITY, SAMPLING, AND APPLICATION OF A DNA-TAGGED TRACER FOR AEROSOL TRANSPORT STUDIES

By

Cynthia Jeanne Kaeser

Aerosols are an ever-present part of our daily environment and have extensive effects on both human and environmental health. Particles in the inhalable range (1-10 μm diameter) are of particular concern because their deposition in the lung can lead to a variety of illnesses including allergic reactions, viral or bacterial infections, and cancer. Understanding the transport of inhalable aerosols across both short and long distances is necessary to predict human exposures to aerosols. To assess the transport of hazardous aerosols, surrogate tracer particles are required to measure their transport through occupied spaces. These tracer particles must not only possess similar transport characteristics to those of interest but also be easily distinguished from the background at low levels and survive the environmental conditions of the testing environment. A previously-developed DNA-tagged particle (DNATrax), composed of food-grade sugar and a DNA oligonucleotide as a “barcode” label, shows promise as a new aerosol tracer.

Herein, the use of DNATrax material is validated for use in both indoor and outdoor environments. Utilizing passive samplers made of materials commonly found in indoor environments followed by quantitative polymerase chain reaction (qPCR) assay for endpoint particle detection, particles detection was achieved up to 90 m from the aerosolization location and across shorter distances with high spatial resolution. The unique DNA label and PCR assay specificity were leveraged to perform multiple simultaneous experiments. This allowed the assessment of experimental reproducibility, a rare occurrence among aerosol field tests. To transition to outdoor testing, the solid material provides some protection of the DNA label when

exposed to ultraviolet (UV) radiation, with 60% of the DNA remaining intact after 60 minutes under a germicidal lamp and the rate of degradation declining with irradiation time. Additionally, exposure of the DNATrax material using formulations of two different food-grade sugars (maltodextrin and erythritol) to humidity as high as 66% had no significant effect on the DNA label's degradation or the particle's aerodynamic diameter, confirming particle stability under such conditions. In summary, confirmation of the DNATrax particles' size and label integrity under variable conditions combined with experiment multiplexing and high resolution sampling provides a powerful experimental design for modeling aerosol transport through occupied indoor and outdoor locations.

ACKNOWLEDGEMENTS

I would like to first thank my research advisor at MSU, Dan Jones, for his mentorship and encouragement throughout the last 7 years. You once told me that successful scientists know when to take risks and I am thankful for your encouragement to take those risks, especially in moving to Lawrence Livermore National Laboratory. Thank you to Elizabeth Wheeler, who has served as my LLNL advisor for the last 2+ years, and to George Farquar for initially recruiting me to the DNATrax project. I must also thank my current committee members, Dana Spence and Gary Blanchard, and my former committee members, Gavin Reid and David Kramer.

Beyond those who have advised me in an official capacity, I must also thank the current and former Jones group members, especially Prabodha, Kristen, and Fanny, and the current and former DNATrax project members for passing along their knowledge and perspective.

I am grateful for the unyielding support of my family and the friends that have become family, especially my California family, Katie, the members of St. Charles, and those that have walked with me in various capacities along the way. I am especially grateful to Thuan for the constant pep talks, perspective, and prayer. I look forward to more life adventures with you.

I would like to acknowledge the funding sources that have supported me and my work throughout graduate school: the MSU Chemistry Department, the LLNL Lawrence Scholar Program, the Defense Threat Reduction Agency, and the Department of Homeland Security. This work was performed under the auspices of the U.S. Department of Energy by Lawrence Livermore National Laboratory under Contract DE-AC52-07NA27344. LLNL-TH-735173.

Thank you to my Lord and God for leading me through this path that is wilder than I could have ever imagined. This has been quite the journey – now, on to the next one!

TABLE OF CONTENTS

LIST OF TABLES	vi
LIST OF FIGURES	ix
CHAPTER ONE: Introduction to Aerosol Transport and Tracers	ix
1.1 Motivation and Scope of Work.....	1
1.2 Transport Study Considerations.....	2
1.3 Development of the Aerosol Tracer DNATrax	4
1.4 Specific Aims.....	8
REFERENCES	9
CHAPTER TWO: Multiplexed Indoor Aerosol Transport Determination Using DNA- Barcoded Aerosols and Passive Sampling.....	13
2.1 Introduction.....	13
2.1.1 Indoor Air Hazards	13
2.1.2 Aerosol Tracer Selection.....	14
2.1.3 Aerosol Sampling Techniques	16
2.1.4 Aerosol Field Tests	17
2.1.5 Specific Aims.....	17
2.2 Materials and Methods.....	18
2.2.1 DNATrax Material Preparation	18
2.2.2 Passive Sampling Material Validation.....	19
2.2.3 Field Test Set-ups	20
2.3 Results and Discussion	22
2.3.1 Passive Sampler Validation	22
2.3.2 Single Barcode Testing	24
2.3.3 Multiple Barcode Testing	27
2.4 Conclusions.....	30
APPENDIX.....	31
REFERENCES	36
CHAPTER THREE: Stability of DNATrax Material as a Function of Exposure to UV Radiation.....	39
3.1 Introduction.....	39
3.1.1 Photodegradation Mechanisms	39
3.1.2 Specific Aims.....	43
3.2 Materials and Methods.....	43
3.2.1 Material Production and DNA Analysis	43
3.2.2 UV Degradation Under Germicidal Lamp.....	45
3.2.3 Gel Electrophoresis Analysis.....	46
3.3 Results and Discussion	47
3.3.1 DNA Degradation Determination using qPCR.....	47

3.3.2 Degradation Products Analysis by Gel Electrophoresis (GE) and qPCR.....	53
3.3.3 Degradation Mitigation.....	58
3.4 Conclusions.....	59
APPENDIX.....	61
REFERENCES	64
CHAPTER FOUR: Stability of DNATrax Material as a Function of Exposure to Humidity	67
4.1 Introduction.....	67
4.1.1 Hygroscopicity of Sweeteners	67
4.1.2 Particle Size and Aerosol Transport	69
4.1.3 DNA Degradation Mechanisms.....	72
4.1.4 Specific Aims.....	73
4.2 Materials and Methods.....	73
4.2.1 Solid Material Production Conditions	73
4.2.2 Particle Size Determination	74
4.2.3 Humidity Chamber Set-up	75
4.2.4 Humidity Chamber Incubation	76
4.3 Results and Discussion	77
4.3.1 Particle Production using Alternative Sweeteners.....	77
4.3.2 Effect of Humidity Exposure on Bulk Weight	78
4.3.3 Effect of Humidity Exposure on Particle Size.....	82
4.3.4 Effect of Humidity Exposure on DNA Degradation.....	86
4.4 Conclusions.....	89
APPENDIX.....	91
REFERENCES	96
CHAPTER FIVE: Conclusions	99

LIST OF TABLES

Table 2.1 Spray drying parameters for the production of DNATrax material.	19
Table 2.2 Protocols for the a) master mix and b) thermal profile used with the PCR analysis.	19
Table 2A.1 Average cycle threshold for DNA templates used during the multiple barcode testing with each template’s master mix (1 fg DNA per reaction; n=3 reactions). Combinations in which the fluorescence did not exceed the threshold after 40 cycles are indicated by “N/A.”	32
Table 2A.2 Amount of DNATrax material collected on Post-It® notes and cotton t-shirt samplers (n=1; copies DNA/cm ²) along a 90-m stretch of hallway.	34
Table 2A.3 Average amount and relative standard deviation (RSD) of DNATrax material collected on Post-It® notes (n=3; ng/cm ²) along at 1-m intervals during the second hallway testing.	34
Table 2A.4 Average amount of DNATrax material collected on glass slides (n=3; ng/cm ²) along the cross-sections of the center line during the multiple barcode testing.	35
Table 3.1 Composition of each solid material used for degradation experiments.	44
Table 3.2 Composition of each aqueous solution used for degradation experiments.	44
Table 3A.1 Base composition and length of the double-stranded DNA sequences used for DNATrax labeling and length of the primer and probe sequences.	62
Table 3A.2 Average relative concentrations of Barcode A DNA in solid DNATrax particles and aqueous solutions both with and without Fluorescent Brightener 220 as a function of irradiation time, assessed using qPCR. Standard deviations are the three replicate samples irradiated simultaneously.	62
Table 3A.3 Average relative concentrations of Barcode B DNA in solid DNATrax particles and aqueous solutions as a function of irradiation time, assessed using qPCR. Standard deviations are the three replicate samples irradiated simultaneously.	63
Table 4.1 Physical properties and chemical structure of commercially available sweeteners with low hygroscopicity.	68
Table 4.2 Incubation location for the rotation, high, low, and ambient aliquots during the hygroscopicity study.	77

Table 4A.1 Changes in bulk weight relative to the starting weight for maltodextrin material. Averages and standard deviations are for n=3 aliquots.93

Table 4A.2 Changes in bulk weight relative to the starting weight for erythritol material. Averages and standard deviations are for n=3 aliquots.93

Table 4A.3 Average MMAD values for maltodextrin material. Averages and standard deviations are for n=3 aliquots.93

Table 4A.4 Average d90 values for maltodextrin material. Averages and standard deviations are for n=3 aliquots.94

Table 4A.5 Average MMAD values for erythritol material. Averages and standard deviations are for n=3 aliquots.94

Table 4A.6 Average d90 values for erythritol material. Averages and standard deviations are for n=3 aliquots.....94

Table 4A.7 Copies of DNA per 2- μ m particle of maltodextrin-based DNATrax as determined using qPCR. Averages and standard deviations are for n=3 aliquots.95

Table 4A.8 Copies of DNA per 2- μ m particle of erythritol-based DNATrax as determined using qPCR. Averages and standard deviations are for n=3 aliquots.....95

LIST OF FIGURES

Figure 1.1 Schematic of the spray dryer indicating the flows of both the gas and liquid as well as the temperature measurement points. The air flow heating and cooling is indicated by the color of the arrows.	5
Figure 1.2 Summary of DNA replication in a polymerase chain reaction (PCR).	7
Figure 1.3 a) Determination of cycle threshold in qPCR for known standards (9.89×10^7 copies DNA per reaction to 98.9 copies DNA per reaction) and conversion to b) a calibration curve for the quantification of DNA in a sample (red trace).....	8
Figure 2.1 PCR curves to compare assay inhibition (green circles) and DNA recovery (orange triangles) to control curves (blue diamonds) using a) glass microscope slides and b) Post-It® notes. Inhibition of undiluted samples (solid lines) in the Post-it® notes was mitigated using a 10x dilution of each solution (dashed lines). The fluorescence threshold is denoted by the black line.....	23
Figure 2.2 Amount of DNATrax material deposited at each sampling point along a 90-m stretch of hallway. Collection of material used Post-It® notes and cotton t-shirt squares (n=1 each). Numerical values for each data point can be found in Table 2A.2.....	25
Figure 2.3 a) Amount of DNATrax material deposited at each sampling point along a hallway. Collection of material used Post-It® notes (n=3). The error bars indicate the standard deviation for the average amount collected. b) Schematic of release hallway on the same scaling as the data in a). Air flow varied from 0.2 to 0.5 m·s ⁻¹ along the length of the hallway at approximately 1.5 m above the floor. Numerical values for each data point can be found in Table 2A.3.	26
Figure 2.4 Average amount of DNATrax material collected on glass slides (n=3) along the cross-sections of the center line in a) the Mix 1 (A/B) direction and b) the Mix 2 (C/D) direction. Error bars indicate the standard deviation for the average amount collected on the glass slides. c) Schematic of testing location. Numerical values for each data point can be found in Table 2A.4.	29
Figure 2A.1 Aerodynamic size distributions for DNATrax material of each label used during the multiple barcode testing.	32
Figure 2A.2 PCR fluorescence curves for control (blue), inhibition (green), and recovery (orange) DNA solutions for the passive sampling materials a) polyester filter, b) glass slide, c) t-shirt cotton, d) filter paper, e) Post-It® note and f) Post-It® note with a 10x dilution. The threshold value is indicated by the black line.	33
Figure 3.1 The pyrimidine base a) thymine and two products of photoinduced crosslinking of adjacent thymine monomers: b) 6,4-photoproduct and c) cyclobutane dimer.....	40

Figure 3.2 Summary of photooxidation reaction mechanisms.	41
Figure 3.3 Formation of 8-oxo-7,8-dihydroguanine a) through ionization and reaction with water or oxygen and b) through reaction with singlet oxygen.	42
Figure 3.4 Intensity factors for light emitted across UV and visible wavelengths for the germicidal lamp used, as provided by the manufacturer.	45
Figure 3.5 Average relative concentrations of DNA Barcode A sequence in solid DNATrax material and aqueous solutions both with and without Fluorescent Brightener 220 as a function of irradiation time, assessed using qPCR. Error bars indicate the standard deviation of three replicate samples irradiated simultaneously. Numerical values for this data is found in Table 3A.2.....	48
Figure 3.6 Ratio of the average a) natural log and b) inverse of the amplifiable DNA Barcode A sequence in aqueous solutions by qPCR after UV exposure to the amount of DNA present with no exposure. The error bars indicate the standard deviations of triplicate samples. The best fit lines for the data, forced through an intercept of 1, are also shown.	51
Figure 3.7 Ratio of the average a) natural log and b) inverse of the amplifiable DNA Barcode A sequence in solid material by qPCR after UV exposure to the amount of DNA present with no exposure. The error bars indicate the standard deviations of triplicate samples. The best fit lines for the data, forced through an intercept of 1, are also shown.....	52
Figure 3.8 GE results of aqueous DNA (Aq) and solid material with DNA labeling (High and Low), after varying lengths of irradiation with no PCR amplification prior to GE analysis. Serial dilutions of a standard aqueous DNA solution (Std Aq) as well as a DNA ladder (DNA Lad) are included for reference. The image is shown both a) as acquired at the time of analysis and b) after adjustment of the brightness scale to improve visualization of low intensity bands, highlighted using the black box, using Adobe PhotoShop.	54
Figure 3.9 Average pixel brightness of horizontal pixels across a GE lane as a function of migration distance for UV-degraded samples of the Barcode A-labelled solid with high DNA labeling. All data have been background subtracted.	55
Figure 3.10 Fraction of DNA Barcode A sequence remaining quantified through qPCR as well as through GE with image brightness analysis for a) aqueous DNA, b) solid material with a high level of DNA labeling, and c) solid material with a low level of DNA labeling.....	56
Figure 3.11 Average relative concentrations of either the Barcode A sequence (blue traces) or Barcode B sequence (orange traces) of DNA in a) solid DNATrax particles and b) aqueous solutions as a function of irradiation time, assessed using qPCR. Standard deviations are the three replicate samples irradiated simultaneously. Numerical data for these graphs can be found in Table 3A.3.	59

Figure 4.1 Example of a lognormal distribution of particle size plotted a) by the fraction of the total number of sample counts at each aerodynamic diameter and b) by the fraction of the total mass of particles represented by particles of each aerodynamic diameter. The mass median aerodynamic diameter (MMAD) and 90th mass percentile (d90) are marked in panel b.72

Figure 4.2 Diagram of the aerosol generation and sizing method used.....75

Figure 4.3 Change in bulk weight of a) maltodextrin-based or b) erythritol-based DNATrax material in response to c) the relative humidity in each chamber. Error bars indicate the standard deviations of triplicate samples. Numerical values for bulk weights can be found in Tables 4A.1 and 4A.2.80

Figure 4.4 Average aerodynamic diameter of maltodextrin-based particles assessed using a) the MMAD and b) the d90 after incubation at high humidity, low humidity, or both on a rotating basis according to the c) humidity profiles. Error bars indicate the standard deviation of triplicate samples. Numerical values for bulk weights can be found in Tables 4A.3 and 4A.4.84

Figure 4.5 Average aerodynamic diameter of erythritol-based particles assessed using a) the MMAD and b) the d90 after incubation at high humidity, low humidity, or both on a rotating basis according to the c) humidity profiles. Error bars indicate the standard deviation of triplicate samples. Numerical values for bulk weights can be found in Tables 4A.5 and 4A.6.85

Figure 4.6 Copies of replicable DNA per particle with a 2- μ m aerodynamic diameter in maltodextrin-based and erythritol-based DNATrax material as determined by qPCR after storage at low humidity, high humidity, rotation between low and high humidity, or ambient conditions. Error bars are the standard deviation of 3 samples. Significant differences between DNA levels are indicated by the brackets (95% confidence).87

Figure 4.7 Relative humidity experienced by aliquots stored in high- or low-humidity chambers, rotated between them, or stored on the benchtop under ambient condition.89

Figure C.1 Particle size distributions for maltodextrin and erythritol-based DNATrax plotted as the a) physical diameter scaled by counts, b) aerodynamic diameter scaled by counts, and c) aerodynamic diameter scaled by mass.92

CHAPTER ONE: Introduction to Aerosol Transport and Tracers

1.1 Motivation and Scope of Work

Aerosols are solid particulates or liquid droplets dispersed in the air and can be either naturally-occurring (*e.g.* fog, pollen, salt from ocean spray) or anthropogenic (*e.g.* combustion products, smoke). While some aerosols have environmental effects such as aiding cloud nucleation or forming a “haze” that inhibits cloud formation and suppresses precipitation¹, aerosols are also associated with a range of health effects, including allergic reaction to pollens, infection from viral or bacterial pathogens, and cancer due to combustion and smoking byproducts². Spending time indoors does not inherently minimize aerosol exposure, with molds and microbial growth affecting the health of building inhabitants and leading to instances of “sick building syndrome”³. However, the ability of aerosols to penetrate the human lung is not inherently negative as a range of pharmaceuticals treatments from asthma medications to sedatives are administered by aerosolization and inhalation⁴.

While aerosols are generated from a broad range of sources and provide a variety of effects, the scope of this work will focus on the transport properties of aerosols in the range of human inhalation. A particle’s transport through air and subsequent deposition in the lung depends on a variety of factors including the particle’s size, shape, charge, density and hygroscopicity⁵. However, in general, particles less than 10 μm in aerodynamic diameter can penetrate the alveolar region of the lung with 1-5 μm particles having the highest deposition rate in that region⁶. Common aerosols in this size range include some pollens and animal dander, bacteria, cooking aerosols, and dust⁷.

1.2 Transport Study Considerations

While personal aerosol sampling can monitor aerosol exposure as it occurs, it is also valuable to predict the particle transport that leads to exposure when a release of aerosols is expected, as in cases of occupational exposures. Computational models provide the basis for such predictions and have been used to predict aerosol transport in both small air volumes, such as within an aerosol sampler⁸ or human airways⁹, to larger volumes such as cross-country distances¹⁰⁻¹². Models have also been used to assess particle transport in indoor rooms with varying layouts and levels of occupation¹³⁻¹⁷. While they are extensively used, the validation of transport models is plagued by a lack of clear definitions as to how models should be validated and the minimal requirements for refining such models through experimental testing¹⁸.

Experimental investigation of particle transport has been performed through monitoring of either indigenous aerosols or material aerosolized for the sole purpose of the experiment. While investigating transport of aerosols that affect human health, it is advantageous to use a non-hazardous surrogate for the aerosol of interest, such as an aerosol tracer. Aerosol tracers can be used to model the transport of hazardous aerosols in locations where it is not feasible to use the hazardous aerosols. These surrogates must have transport characteristics similar to the aerosol of interest, be easily distinguished from aerosols already present, be safe for human exposure with little or no decontamination necessary before the space can be reoccupied, and be stable under the environmental conditions of the experiment¹⁹. Aerosol tracers in the inhalable range have utilized both biological-based particles (*e.g.* bacteria spores^{20,21}) and man-made particles (*e.g.* polymer or silica spheres^{22,23}) with either fluorescent or DNA-based detection schemes providing sensitivity needed to measure individual aerosol particles. While each tracer offers its own advantages, DNA-based detection schemes, including real-time quantitative polymerase chain

reaction (qPCR), offer low detection limits and quantification of individual components²⁴.

Detection limits as low as single-digit particle counts for an aerosol tracer, even in locations with a high level of background aerosols present, is a primary advantage of using an aerosol tracer with a unique fluorescent or DNA identifier over using indigenous aerosols.

For experimental validation of transport in indoor environments, using a test chamber is often preferred over an occupied space, as transport studies performed outside of an enclosed test chamber provide have less control over the characteristics of the environment¹⁴. Some of these characteristics, such as light and humidity exposure, have the potential to alter the detectability or transport properties of an aerosol. Light exposure can lead to photobleaching of fluorophores or degradation of DNA in aerosol tracers, increasing the lower limits of detection. For hygroscopic materials, fluctuations in the humidity can alter the amount of adsorbed water, leading to alterations in particle mass and potential issues with agglomeration. Thus, to accurately assess aerosol transport using an aerosol tracer, the stability of the aerosol tracer with respect to these variables must be understood.

An additional, often overlooked, concern in transport studies is the reproducibility of results. With constant variation in the environment, guaranteeing that replicate studies are under identical conditions from the moment of aerosolization to collection requires that the studies be performed simultaneously. Based on the ability of the qPCR assay to quantify specific DNA sequences from a mixture, a DNA-tagged tracer material may be a suitable platform for performing aerosol transport reproducibility studies as well.

1.3 Development of the Aerosol Tracer DNATrax

Leveraging the power of DNA detection schemes with the safety of food-grade materials, an aerosol tracer was developed. This tracer, denoted DNATrax (DNA-Tagged Reagent for Aerosol eXperiments), paired unique double-stranded DNA sequences (dsDNA) with organic, food-safe sweeteners as the bulk material. Original production utilized the sugar glucono-delta-lactone (GDL) with inkjet printing for particle production²⁵, but an alternate production scheme using maltodextrin, a sugar with a higher glass transition temperature than GDL, and a commercially available spray dryer resulted in the gram-scale production necessary for aerosol releases in larger spaces²⁶. The spray drying process, summarized in Figure 1.1²⁵, begins by spraying an aqueous solution as fine droplets into a heated airstream. The droplets rapidly dry in the airstream, condensing the materials dissolved in the aqueous solution into a solid particle. The solid particles are collected by impaction on the walls of the collection cyclone and drop into the collection chamber.

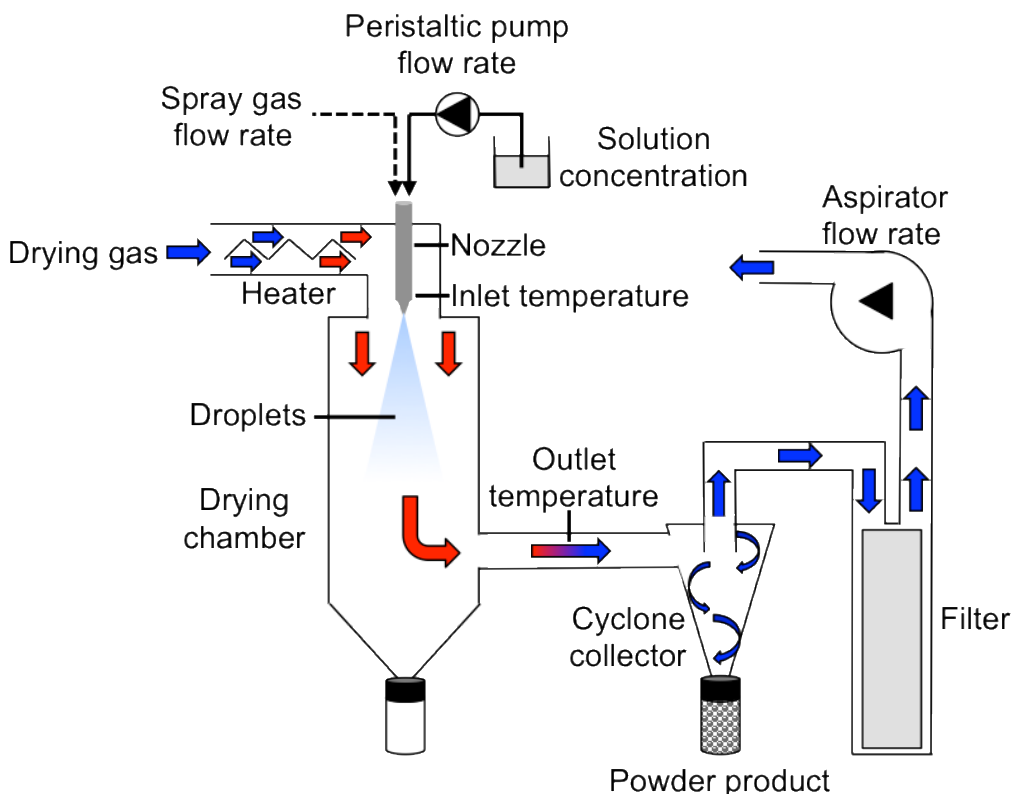
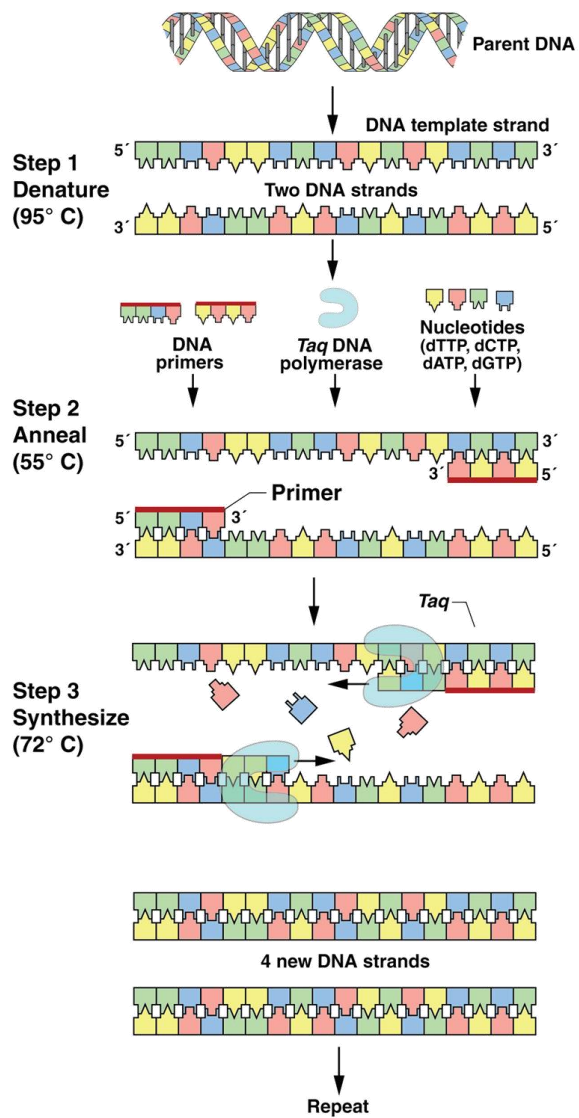


Figure 1.1 Schematic of the spray dryer indicating the flows of both the gas and liquid as well as the temperature measurement points. The air flow heating and cooling is indicated by the color of the arrows.

After production, detection and quantification of the DNA label in the powder is performed using qPCR, a process summarized in Figure 1.2. In qPCR, the double-stranded DNA oligonucleotides are denatured and complementary strands synthesized. This theoretically doubles the copies of dsDNA with each thermal cycle, with a single parent dsDNA strand yielding 1.1 billion copies of DNA after 30 cycles through the process. In addition to the use of sequence-specific primers that allow amplification of a single dsDNA sequence even when multiple sequences are present, the addition of a sequence-specific fluorescent probe provides the basis for DNA quantification. The probe is a short (~20 bp) oligonucleotide sequence that is complementary to one of the dsDNA strands with a fluorophore (6-FAM; fluorescein) at the 5'-

end and a quencher (Black Hole Quencher®-1) at the 3'-end. During the strand synthesis step, the fluorescent probe is cleaved from the oligonucleotide. With increased distance between the fluorophore and the quencher, the fluorophore's fluorescence can be detected. The intensity of fluorescence within the solution is directly proportional to the number of dsDNA strands produced, doubling with each cycle. For each fluorescence curve, a threshold cycle (Ct) is defined as the PCR cycle at which the fluorescence intensity passes a set threshold, for known DNA concentrations (Figure 1.3a). There is a linear relationship between the cycle threshold and number of DNA copies at the start of the PCR cycling (Figure 1.3b). This allows quantification of DNA in a solution of unknown concentration using a calibration curve of solutions of known DNA concentrations. Thus, for quantification of particle transport in a field test, the ratio of DNA content per mass of DNATrax material assessed prior to an experiment is compared with the DNA content collected at various locations across the test space.

The DNATrax material posits several advantages as an aerosol tracer. First, its synthetic DNA tag and food-grade bulk material provide a low burden of approval for testing in occupied spaces. Also, by using unique DNA sequences, each batch of material produced can have a different signature that is easily separated from both background aerosols and DNATrax particles containing other sequences. This provides a platform for multiplexed experiments, allowing multiple variables to be investigated simultaneously as well as assessing the reproducibility of an experiment's results. However, to serve as a tracer for outdoor environments, the bulk material and DNA oligonucleotide must be stable under the variable humidity and light exposures for the duration of the experiment.



Z-1296-06

Figure 1.2 Summary of DNA replication in a polymerase chain reaction (PCR).

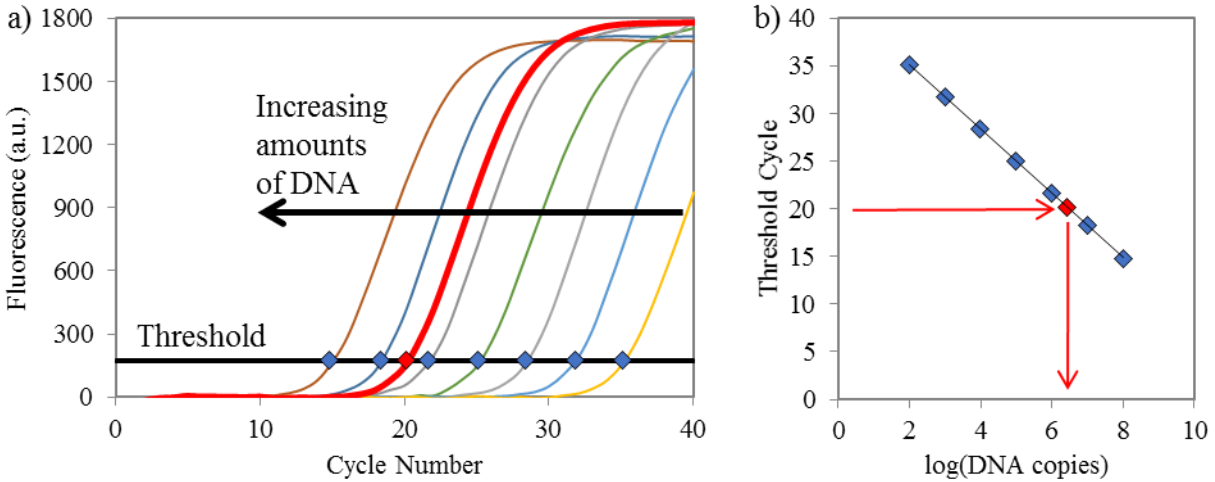


Figure 1.3 a) Determination of cycle threshold in qPCR for known standards (9.89×10^7 copies DNA per reaction to 98.9 copies DNA per reaction) and conversion to b) a calibration curve for the quantification of DNA in a sample (red trace).

1.4 Specific Aims

This work challenges the proposed advantages of using DNATrax material as an aerosol tracer by examining its transport and label stability under a range of indoor and outdoor environments. Chapter 2 details its use indoors, showing the low limits of detection enable detection with passive samplers as far as 90 meters from the point of aerosolization. Using multiple materials each with a unique barcode, the reproducibility of indoor experiments is also assessed. Chapters 3 and 4 discuss the effects of exposure to UV radiation and variable humidity, respectively, on both the DNA tag and the particle size, as these characteristics dictate the particle detection and transport properties.

REFERENCES

REFERENCES

1. Tao W-K, Chen J-P, Li Z, Wang C, Zhang C. Impact of aerosols on convective clouds and precipitation. *Rev Geophys*. 2012. 50: RG2001.
2. Douwes J, Thorne P, Pearce N, Heederik D. Bioaerosol health effects and exposure assessment: progress and prospects. *Ann Occup Hyg*. 2003. 47: 187-200.
3. Walinder R, Norback D, Wessen B, Venge P. Nasal lavage biomarkers: effects of water damage and microbial growth in an office building. *Arch Environ Health*. 2001. 56: 30–36.
4. Stein SW, Thiel CG. The history of therapeutic aerosols: a chronological review. *J Aerosol Med Pulm Drug Deliv*. 2017. 30: 20-41.
5. Schlesinger RB. Comparative deposition of inhaled aerosols in experimental animals and humans: a review. *J Tox and Environ Health*. 1985. 15: 197-214.
6. Byron PR. Prediction of drug residence times in regions of the human respiratory tract following aerosol inhalation. *J Pharm Sci*. 1986. 75: 433–438.
7. Brain JD, Valberg PA. Deposition of aerosol in the respiratory tract. *Am Rev Respir Dis*. 1979. 120: 1325-1373.
8. Sajjadi H, Tavakoli B, Ahmadi G, Dhaniyala S, Harner T, Holsen TM. Computational fluid dynamics (CFD) simulation of a newly designed passive particle sampler. *Environ Pollut*. 2016. 214: 410-418.
9. Oldham MJ. Computational fluid dynamic predictions and experimental results for particle deposition in an airway model. *Aerosol Sci Technol*. 2000. 32: 61-71.
10. Owega S, Khan BUZ, Evans GJ, Jervis RE, Fila M. Identification of long-range aerosol transport patterns to Toronto via classification of back trajectories by cluster analysis and neural network techniques. *Chemometr Intell Lab*. 2006. 83: 26-33.
11. Chin M, Diehl T, Ginoux P, Malm W. Intercontinental transport of pollution and dust aerosols: implications for regional air quality. *Atmos Chem Phys*. 2007. 7: 5501-5517.
12. Wong MS, Nichol JE, Lee KH. Estimation of aerosol sources and aerosol transport pathways using AERONET clustering and backward trajectories: a case study of Hong Kong. *Int J Remote Sens*. 2013. 34: 938-955.

13. Tao Y, Inthavong K, Petersen P, Mohanarangam K, Yang W, Tu J. Experimental and CFD modelling of indoor air and wake flow from a moving manikin. *20th Australasian Fluid Mechanics Conference*. 2016.
14. Sajjadi H, Salmanzadeh M, Ahmadi G, Jafari S. Simulations of indoor airflow and particle dispersion and deposition by the lattice Boltzmann method using LES and RANS approaches. *Build Environ*. 2016. 102: 1-12.
15. Lu W, Howarth AT, Adams NM, Riffat SB. CFD modeling and measurement of aerosol particle distributions in ventilated multizone rooms. *ASHRAE Trans*. 1999. 105, part 2: 116-127.
16. Sohn MD, Apte MG, Sextro RG, Lai ACK. Predicting size-resolved particle behavior in multizone buildings. *Atmos Environ*. 2007. 41: 1473-1482.
17. Richmond-Bryant J, Eisner AD, Bixey LA, Wiener RW. Transport of airborne particles within a room. *Indoor Air*. 2006. 16: 48-55.
18. Oldham MJ. Challenges in validating CFD-derived inhaled aerosol deposition predictions. *Inhal Toxicol*. 2006. 18: 781-786.
19. Sinclair RG, Rose JB, Hashsham SA, Gerba CP, Haas CN. Criteria for selection of surrogates used to study the fate and control of pathogens in the environment. *Appl Environ Microbiol*. 2012. 78: 1969-1977.
20. Emanuel PA, Buckley PE, Sutton TA, Edmonds JM, Bailey AM, Rivers BA, Kim MH, Ginley WJ, Keiser CC, Doherty RW, Kragl FJ, Narayanan FE, Katoski SE, Paikoff S, Leppert SP, Strawbridge JB, VanReenen DR, Biberos SS, Moore D, Phillips DW, Mingioni LR, Melles O, Ondercin DG, Hirsh B, Bieschke KM, Harris CL, Omberg KM, Rastogi VK, Cuyk SV, Gibbons HS. Detection and tracking of a novel genetically tagged biological simulant in the environment. *Appl Environ Microb*. 2012. 78: 8281-8288.
21. King MF, Noakes CJ, Sleigh PA, Camargo-Valero MA. Bioaerosol deposition in single and two-bed hospital rooms: a numerical and experimental study. *Build Environ*. 2013. 59: 436-447.
22. Liljegren JC, Brown DF, Lunden MM, Silcott D. Particle deposition onto people in a transit venue. *Health Security*. 2016. 14: 237-249.
23. Lai ACK, Byrne MA, Goddard AJH. Experimental studies of the effect of rough surfaces and air speed on aerosol deposition in a test chamber. *Aerosol Sci Technol*. 2002. 36: 973-982.
24. Lopez-Andreo M, Lugo L, Garrido-Petierra A, Preito MI, Puyet A. Identification and quantitation of species in complex DNA mixtures by real-time polymerase chain reaction. *Anal Biochem*. 2005. 339: 73-82.

25. Udey RN, Jones AD, Farquar G R. Aerosol and microparticle generation using a commercial inkjet printer. *Aerosol Sci Technol.* 2013. 47: 361-372.
26. Harding RN, Hara CA, Hall SB, Vitalis EA, Thomas CB, Jones AD, Day JA, Tur-Rojas VR, Jorgensen T, Herchert E, Yoder R, Wheeler EK, Farquar GR. Unique DNA-barcoded aerosol test particles for studying aerosol transport. *Aerosol Sci Technol.* 2016. 50: 429-435.

CHAPTER TWO: Multiplexed Indoor Aerosol Transport Determination Using DNA-Barcoded Aerosols and Passive Sampling

2.1 Introduction

Accurate assessment and prediction of indoor health hazards posed by exposure to aerosols in the respirable range (1-10 μm) requires an understanding of particle transport in occupied spaces. Occupied spaces present several constraints when conducting aerosol releases including, 1) concerns for the safety of the occupants, 2) maintaining the integrity of the test space's HVAC air flow, and 3) the necessity for experimental replicates that can be distinguished. DNA Tagged Reagents for Aerosol eXperiments (DNATrax), a safe simulant with tunable DNA barcodes, provides a platform to overcome these constraints. Coupled with passive sampling, multiple DNATrax materials were used simultaneously to assess both the reproducibility of aerosol transport and the effect of aerosol release direction on the dispersion pattern in an occupied space.

2.1.1 Indoor Air Hazards

Indoor air pollutants such as mold spores, allergens, and bacteria can cause negative immediate and long-term health effects¹. Of most concern are those pollutants with sizes in the respirable range (1-10 μm aerodynamic diameter), as these are capable of entering the lungs and are impacted onto the airway surfaces without being exhaled². Heating, ventilation and air conditioning (HVAC) systems filter out such airborne hazards while also providing air circulation and indoor/outdoor air mixing to maintain indoor air quality. To improve indoor ventilation systems, the manner in which these systems affect aerosol transport through indoor

spaces must be better understood. The observation and prediction of aerosol particle dispersion and deposition patterns in occupied areas is limited by complex and dynamic airflows that provide a changing set of underlying variables which influence particle motion³. The presence of furniture and people add additional complexities to the air movement. While test chambers offer control of these variables, such experiments are not always feasible. Passive sampling of an aerosol simulant released in a test space bridges the gap between the laboratory and the field as it allows testing in occupied locations while introducing as few extra variables as possible. Under uncontrolled airflow conditions, the challenge of assessing the reliability and reproducibility of dispersion is overcome by using multiple samplers at each test site and simultaneous performance of multiple experiments, *e.g.* with different particle sizes or types or releases from multiple locations.

2.1.2 Aerosol Tracer Selection

Aerosol tracers are used in chamber and field aerosol dispersion studies to monitor and predict the transport of aerosols. An ideal tracer would have similar size and transport properties to the aerosol of interest, be easily distinguished from aerosols already present, and be safe for human exposure with little or no decontamination necessary before the space can be reoccupied⁴. Additionally, for multiple simultaneous experiments to be successful, the tracers released must also be distinguishable from each other without having altered transport properties.

Several aerosol tracers have been used in previous studies. The tracer gas sulfur hexafluoride⁵ is nontoxic and can be accurately measured at low concentrations. However, these molecules are smaller in size than the inhalable range particles and will be more affected by Brownian motion. Thus, it is useful for modelling gas transport, but does not provide an accurate

assessment of particle transport. Bacterial spores⁶⁻⁷ are of a more appropriate size, falling within the 1-10 μm range, but fluorescence detection may be unable to distinguish these spores from biological aerosols already present and lack the ability to tune the fluorescence spectrum so multiple experiments can be simultaneously performed. DNA-based detection schemes such as real-time quantitative polymerase chain reaction (qPCR) offer an alternative to fluorescence that allows quantification of trace levels of different DNA markers from a mixture of collected particles⁸. Bacteria with tunable DNA barcodes have been reported⁶ but still suffer from a negative public perception of their safety in occupied spaces. Leveraging the advantages of qPCR detection without the connotations of bacteria, the aerosol simulant material DNATrax (DNA Tagged Reagents for Aerosol eXperiments)⁹ provides an alternative aerosol tracer. DNATrax are sugar-based particles tagged with unique and tunable DNA barcodes. These are spherical particles with aerodynamic diameters within the inhalable range so their transport is representative for the indoor health hazards listed above. Each batch of DNATrax is labelled with a batch-specific DNA sequence as a barcode for detection by a quantitative real-time polymerase chain reaction (qPCR) assay. By using multiple DNATrax batches, each with a differing DNA barcode, DNATrax material released during multiple simultaneous experiments can be collected on the same samplers. The amount of each DNA label collected per sampler is determined at the end of the experiment by qPCR and is not influenced by other DNA sequences present. Utilizing several DNATrax materials each with a differing barcode allows simultaneous releases to be performed and the initial release conditions of each detected particle to be known.

2.1.3 Aerosol Sampling Techniques

In addition to selection of the aerosol tracer, an appropriate sampling technique must also be determined. Aerosol sampling techniques can be classified as either active samplers, which employ vacuum systems to draw air into the sampler, or passive samplers, which rely on deposition through gravitational settling or impaction. With their ability to condense aerosols from large volumes of air into a single measurement, active samplers are most useful when the tracer is at a low concentration¹⁰. However, because they draw in large volumes of air, these samplers alter the airflow of the test space and are impractical when high spatial resolution is desired. Passive sampling techniques have much lower sampling rates, relying on the direct deposition of particles onto the sampler for detection, but preserve the natural air movements in a test space. These samplers are usually small (<100 cm²) and can provide high spatial resolution in when multiple samplers are placed across the test space.

Several aspects should be considered when selecting a passive sampling material. To preserve the authenticity of the sample space, the material selected should be similar to those already found in the testing area, inspiring the use of clean floor tiles⁶ and polyethylene films¹¹ as passive samplers. However, compatibility with the planned detection scheme is vital for an experiment, leading to the use of materials such as glass microscope slides¹², SEM stubs¹³⁻¹⁴, and Petri dishes with growth media⁷. Other desirable qualities in a sampler include durability, portability, and low cost per sampler. Driven by these desirable traits, several potential passive sampling materials were examined to expand the suite of suitable materials to include small, easily manipulated samplers made from materials commonly found in indoor spaces including various cloth and paper textures.

2.1.4 Aerosol Field Tests

Computational models of aerosol transport allow prediction of particle dispersion under a variety of circumstances, but requires validation using experimental data¹⁵. Several previous studies have sought to provide such datasets using a variety of experimental designs including empty rooms with moving mannequins¹⁶, empty rooms with subdivided areas¹⁷⁻¹⁹, and furnished rooms²⁰. However, these transport experiments are typically performed as single experiments of the aerosolization of one tracer under one set of circumstances without any assessment of the experiment reproducibility. For model validation, it would be advantageous to have an assessment of the reproducibility of the experimental set-up from tracer release to collection and quantification to include a level of confidence in the experimental data used. In order to assess the reproducibility of the experimental design, all of the other variables must be held constant, a near impossibility for sequential experiments performed outside of a controlled test chamber. Thus, simultaneous experiments must be performed. With the qPCR assay able to quantitate individual DNA sequences even in mixed samples, multiple DNATrax tracers could be used simultaneously to assess experiment reproducibility. The use of multiple tracers could also be leveraged for multiplexed experiments, distinguishing the effect of multiple release variables (*e.g.* location and direction of release, aerosolization duration, particle size, etc.) under identical environmental conditions.

2.1.5 Specific Aims

The main goal of this work is to validate that the DNATrax aerosol tracer is a suitable tracer for use across long distances (>50 m), over short distances (10 m) with strong airflow, and in cases where simultaneous testing of multiple variables or high spatial resolution sampling is

desired. This validation includes the production and use of DNATrax with differing unique DNA labels, confirmation of the compatibility of prospective passive sampling materials with the qPCR detection scheme, and 3 separate field studies.

2.2 Materials and Methods

2.2.1 DNATrax Material Preparation

Solid DNATrax material was produced via spray-drying using a Mini Spray Dryer B-290 (Büchi; Switzerland), using the parameters listed in Table 2.1^{9,21}. The carrier material was organic food-grade tapioca maltodextrin (DE 10; Ciranda; Thailand) with short synthetic oligonucleotides serving as the DNA label, each approximately 100bp in length. While the standard solutions of each DNA sequence used for calibration curves were purchased (Biosearch Technologies; Petaluma, CA), the stock solutions of DNA used for solid production were from standard DNA solutions previously amplified using a polymerase chain reaction (PCR) assay (Invitrogen; Carlsbad, CA) with sequence-specific primers (Integrated DNA Technologies; Coralville, IA). The components in the qPCR master mix and the thermal profile used for amplification are listed in Table 2.2a and 2.2b, respectively. These qPCR parameters were also used for quantification of DNA concentrations in the solid material and to determine the specificity of the PCR assay with respect to each DNA sequence using standard PCR cross-reactivity analyses (Table 2A.1).

Aspect	Value
Aspirator	475 L/min (70%)
Liquid Flow Rate	9 mL/min (30%)
Nitrogen Flow Rate	13.85 L/min (45mm)
Inlet Temperature	190 °C
Initial Outlet Temperature	110 °C
Solids Concentration (Aq)	3.0% (w/v%)

Table 2.1 Spray drying parameters for the production of DNATrax material.

a) Master Mix	
Reagent	μL
PCR water	14.4
10x Reaction buffer	2.5
50 mM MgCl ₂	1.5
dNTP @ 10 μM	0.5
F/R Primers @ 10 μM	0.5
Probe @ 10 μM	0.5
Platinum Taq	0.1
Sample	5.0

b) Thermal Profile		
Step	Temperature (°C)	Time
1	95	2 minutes
2	95	30 sec
3*	55	30 sec
4	72	30 sec
5	go to step 2 39x (40 cycles total)	
*Optic collection on step 3		

Table 2.2 Protocols for the a) master mix and b) thermal profile used with the PCR analysis.

The size distribution of the resulting particles was assessed by aerosolizing material into a small (1L) test chamber and sampling using an aerodynamic particle sizer (APS) (TSI; Shoreview, MN). The size distributions of all batches were observed to be log normal with aerodynamic diameters ranging from 0.5 to 5 μm with maxima centered between 1 and 2 μm (Figure 2A.1).

2.2.2 Passive Sampling Material Validation

The passive sampling materials investigated in this study represent a variety of materials and textures commonly found in indoor environments, including

- Polyester filters used in dry filter units (Lockheed Martin; Bethesda, MD; round with 4.75 cm diameter),
- Glass microscope slides (Gold Seal; Portsmouth, NH; 2.5 cm by 7.5 cm),
- White cotton t-shirts (Hanes; Winston Salem, NC; cut to 5.1 cm by 5.1 cm),
- Yellow Post-it® notes (3M; Santa Clara, CA; 5.1 cm by 5.1 cm), and
- Grade 1 filter paper (Whatman; Buckinghamshire, UK; round with 11.5 cm diameter).

The extent of matrix inhibition of the PCR assay was determined by extraction of the sampler into PBS (Amresco; Solon, OH) containing 0.1% Triton-X (Acros Organics; Geel, Belgium) and 0.2 pg DNA/ μ L solution. For barcode recovery efficiency, 10 μ L of a 0.2 pg/ μ L solution of aqueous DNA was added directly to each material and allowed to dry before extraction into the buffer and subsequent quantification. All samples and controls were measured in triplicate using the qPCR assay. Inhibition or incomplete recovery was defined as sampler results having a statistically significant shift in the average response curve to more positive cycle threshold (C_t) values relative to the positive control.

2.2.3 Field Test Set-ups

Three field test locations were selected; all indoor occupied spaces controlled by HVAC systems. The HVAC systems were not adjusted before or during the tests to provide an accurate assessment of particle transport under normal operating procedures. All areas were cleared of people apart from those performing the tests, with those present remaining outside of the sampling area from the time of aerosol release until the time of sampler collection.

The first location was a long (>100 m), straight interior hallway. All doors adjacent to the hallway were closed and there were several air vents spaced along the length of the hallway.

DNATrax was aerosolized using an eductor from one end of the hallway in several aliquots totaling 6.85 g of material. The material was passively sampled at 7 locations along the hallway, using three Post-it® notes and three cotton t-shirt squares at each location, set out for the duration of the experiment.

The second location was a shorter hallway measuring 16.0 m long by 1.8 m wide with an overhead air vent at one end and a door opening into an adjacent part of the building at the other. All other doors into the hallway were closed. The DNATrax simulant was aerosolized using an eductor at 2.5 m into the hallway from the open door and approximately 1.5 m above the floor. Aerosolization took place over a period of 10 seconds, dispersing approximately 300 milligrams of material in the direction of the air vent. The hallway air was passively sampled at 1-meter intervals along the hallway for 45 minutes using 3 Post-It® notes at each sampling location. The samplers were then collected and the amount of DNATrax on each sampler was determined using the same procedure for extraction and quantitation used during sampler validation. Note that while the HVAC system was running for the duration of the experiment and provided a definite directional air flow from the vent toward the point of release, the air flow was not specifically controlled during the experiment.

The third location was a larger room (5.9 m by 9.5 m) with one overhead intake air vent and three doors, all remaining closed for the duration of the test. Two batches of barcoded DNATrax material (barcodes A and B) were mixed together and then 110 milligrams of the mixed material was aerosolized from approximately 1.5 m off the ground in the center of the room facing one direction. Fifteen minutes later, 110 milligrams of a second mix of barcodes (C and D) was aerosolized from the same location facing the opposing direction for a total of 220 milligrams of barcoded material aerosolized over the course of the experiment. Each of the

mixed batches was fully aerosolized in under 10 seconds using in-house built eductors with portable carbon dioxide cartridges as a compressed gas source. Sampling was performed at 1-meter intervals along lines perpendicular to the aerosolizing direction with the nearest location being 2.5 m away from the release point in each direction. Three glass slides were used at each location and all samplers were collected 50 minutes after the second release. Similar to the hallway tests, the HVAC system for this room was left on and not specifically controlled.

2.3 Results and Discussion

2.3.1 Passive Sampler Validation

The compatibility of the samplers with PCR was determined by assessing assay inhibition and DNA recovery. As the inhibition, recovery and control samples all have the same concentration of DNA in theory, any significant shift of the cycle threshold for an inhibition or recovery test sample to higher values than the control would indicate inhibition of the assay or incomplete recovery. Figure 2.1a shows the PCR curves for glass slide testing as an example of a sampler that did not inhibit the PCR assay and allowed for complete recovery of DNA (i.e. complete dissolution of the DNATrax material). PCR curves for additional passive sampling materials that passed inhibition and recovery tests (filter paper, polyester filters, and cotton t-shirt fabric) can be found in Figure 2A.2.

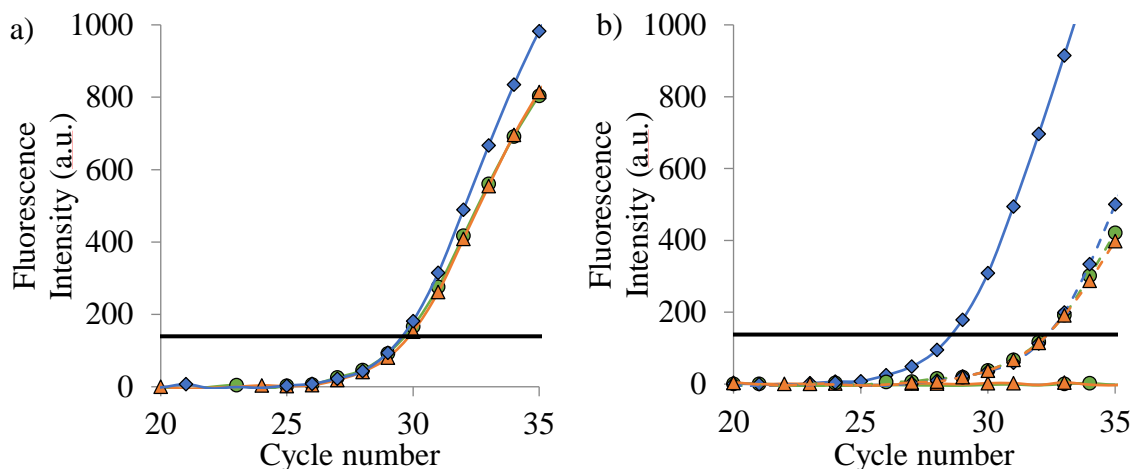


Figure 2.1 PCR curves to compare assay inhibition (green circles) and DNA recovery (orange triangles) to control curves (blue diamonds) using a) glass microscope slides and b) Post-It® notes. Inhibition of undiluted samples (solid lines) in the Post-it® notes was mitigated using a 10x dilution of each solution (dashed lines). The fluorescence threshold is denoted by the black line.

Initial measurements of DNA deposited on Post-It® notes showed no inhibition and complete recovery, but testing with additional packages of the notes yielded evidence of complete inhibition of the PCR assay (Figure 2.1b). However, using 1:10 dilutions of the sample extracts mitigated this effect by diluting the inhibiting compounds and the resulting DNA quantification fell within the assay's margin of error, defined as the standard deviation of three technical replicates. Using this knowledge, the first two field tests were successfully performed using Post-It® notes as passive samplers using the 1:10 dilution before qPCR analysis without sample inhibition. However, while the portability, durability and knowledge that they will not shift position during an experiment are major advantages to using Post-It® notes, the pack-to-

pack variation in inhibition described above is troubling for sampler reproducibility in the long-term. Thus, glass slides were used for the third field test.

2.3.2 Single Barcode Testing

In the first hallway test, particles were successfully detected along the length of the hallway, as far as 90 m from the release location (Figure 2.2) using both Post-It® notes and cotton t-shirt squares. The two sampler types showed similar results at each location along the hallway, with the ratio of copies of DNA between the two sampler types (Post-It® note/T-shirt) ranging from 0.82-1.02. The consistency in amount collected means the two samplers indicates that the sampler composition does not affect its sampling efficiency and these measurements can be considered replicates in sampling for each location. While the sharpest decrease in amount of material collected was from 3 m to 9 m (120 million copies DNA per cm² to 4.7 million copies DNA per cm²) from the release point, there was a gradual decrease of more than two orders of magnitude in DNA levels across the 90 meters. As a point of reference, at 10 copies of DNA per 2-µm particle, the 120 million copies of DNA per cm² at the 3-m location would equate to approximately 50 µg of solid material collected per cm², while the 4.7 million copies of DNA per cm² is approximately 2.0 µg solid material per cm². The successful collection and detection of DNATrax material as far as 90 m from the release point demonstrates DNATrax's usefulness for passively monitoring aerosol transport across large areas. Given that the samplers set out 90 m from the release point still collected a substantial amount (360,000 copies DNA per cm²; 0.15 µg solid material per cm²) of DNATrax material, small particles with longer residence time travelled further, which indicates potential for studies involving even greater distances.

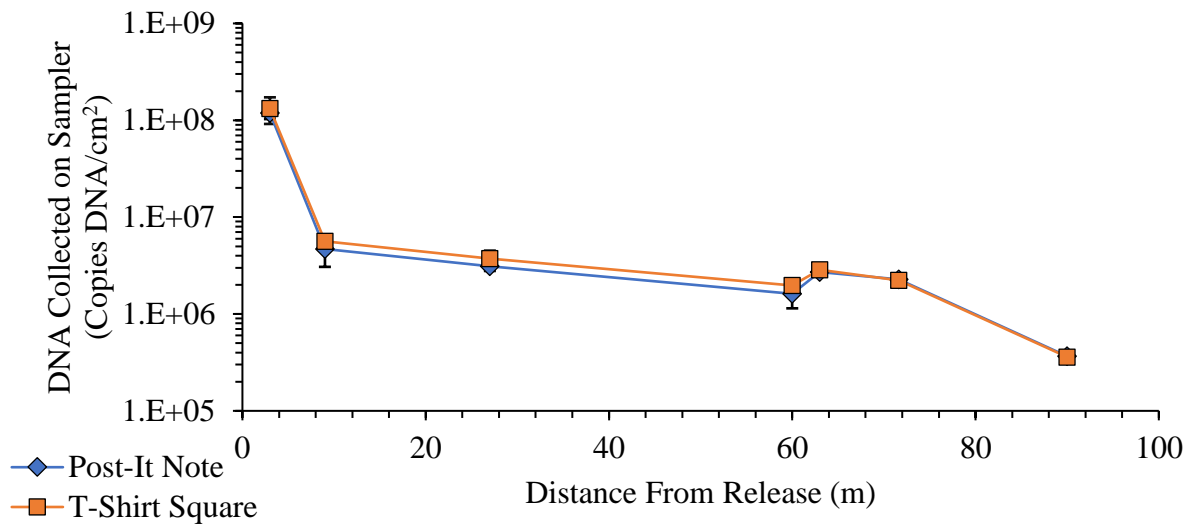


Figure 2.2 Amount of DNATrax material deposited at each sampling point along a 90-m stretch of hallway. Collection of material used Post-It® notes and cotton t-shirt squares (n=3 each; error bars represent standard deviation). Numerical values for each data point can be found in Table 2A.2.

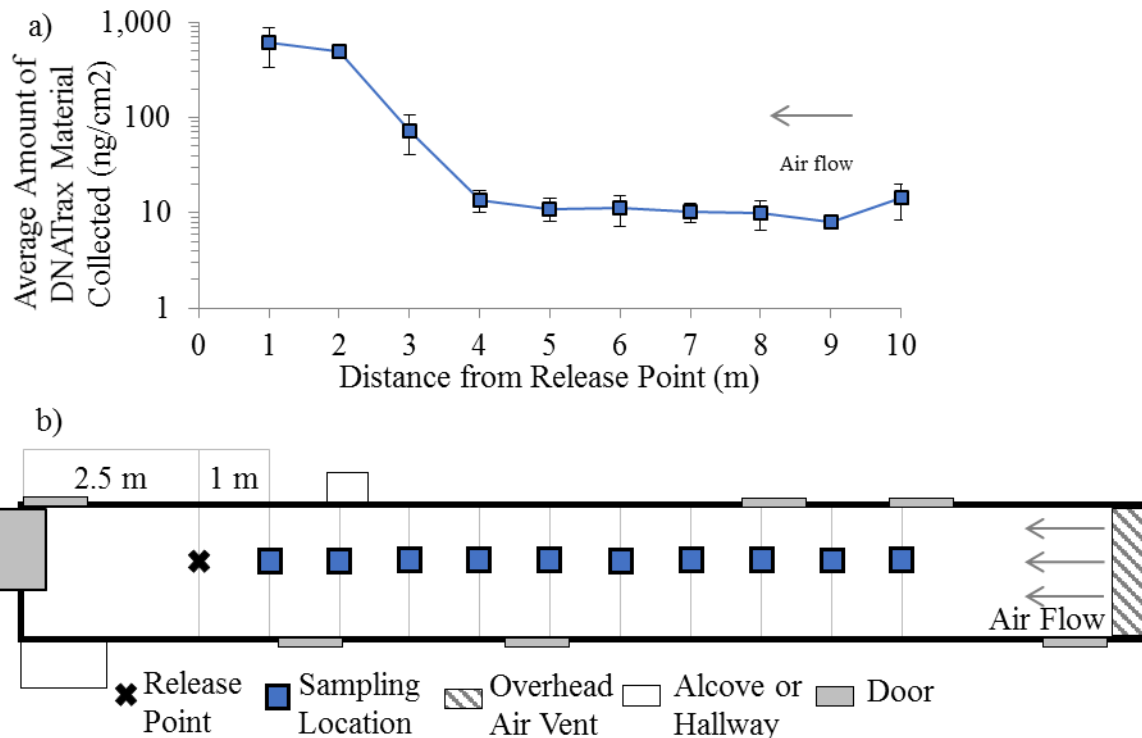


Figure 2.3 a) Amount of DNATrax material deposited at each sampling point along a hallway. Collection of material used Post-It® notes (n=3). The error bars indicate the standard deviation for the average amount collected. b) Schematic of release hallway on the same scaling as the data in a). Air flow varied from 0.2 to 0.5 m·s⁻¹ along the length of the hallway at approximately 1.5 m above the floor. Numerical values for each data point can be found in Table 2A.3.

While the first field test demonstrated the distance across which studies can be performed, the second hallway field test aimed to demonstrate sampling with improved spatial resolution. Thus, this test used a much shorter hallway, less released material, and sampling with 1-meter spatial resolution. The amount of solid DNATrax material deposited on samplers along the hallway (in nanograms) spanned nearly 2 orders of magnitude per square centimeter sampled (Figure 2.3a), a decrease similar to that seen across the first 10 meters of the longer hallway study. The steep decrease in amount collected between 2 and 4 m from the release location and

subsequent leveling off to a constant level is consistent with visual observations during the experiment. After aerosolization, a visible cloud of material was observed moving in the direction of release (against the airflow), indicating that the initial aerosol velocity was higher than the HVAC air movement in the hallway. This allowed the particles to travel a short distance before particles decelerated to the ambient air flow conditions defined by the HVAC system and stopped moving down the hallway. This hypothesis is supported by the sharp particle decrease at ~4 m in Figure 2.3a.

Having acquired multiple samples at each location, statistical analysis was used to divide the hallway into 3 zones of distinct exposure amounts. Using a student's t-test with a 95% confidence level, the first two locations away from the release point were found to be statistically similar to each other, but different from all other locations. The location 3 m from the release point was also statistically different from locations 4-10, which were indistinguishable from one another. Thus, the hallway might be divided into areas of high exposure (up to 2 meters from release, ~500-600 ng-cm⁻² DNATrax), moderate exposure (2 to 4 meters from release, ~70 ng-cm⁻² DNATrax) and low exposure (4 or more meters from release, <15 ng-cm⁻² DNATrax). Thus, when considering the exposure of a person to an indoor health hazard, the person's proximity to the point of aerosolization is of great importance.

2.3.3 Multiple Barcode Testing

Passive sampling with high spatial resolution is a powerful tool for observing differences in particle deposition across a test space and the use of replicate samplers at each location adds confidence to the results. To further leverage these advantages when air flow fluctuations within the test space are likely, multiple experiments were performed simultaneously. Identical release

conditions were accomplished by mixing particles of two different DNATrax barcodes and dispersing the mixed material. In doing this, particles of both barcodes in a “mix” are exposed to the same conditions through the duration of the test. Two sets of mixed barcodes (Mix 1 and Mix 2) were released so particles of 4 distinct barcode sequences were present (barcodes A, B, C, and D). In both mixed barcode releases (Figure 2.4), the ratio between levels of the two barcodes remained constant across all locations before and after the release with a Mix 1 (A/B) ratio of 1.49 ± 0.10 and a Mix 2 (C/D) ratio of 1.45 ± 0.16 , by weight. This consistency between barcodes indicates the particle deposition observed at different locations is independent of barcode and highlights the experimental reproducibility inherent with DNATrax.

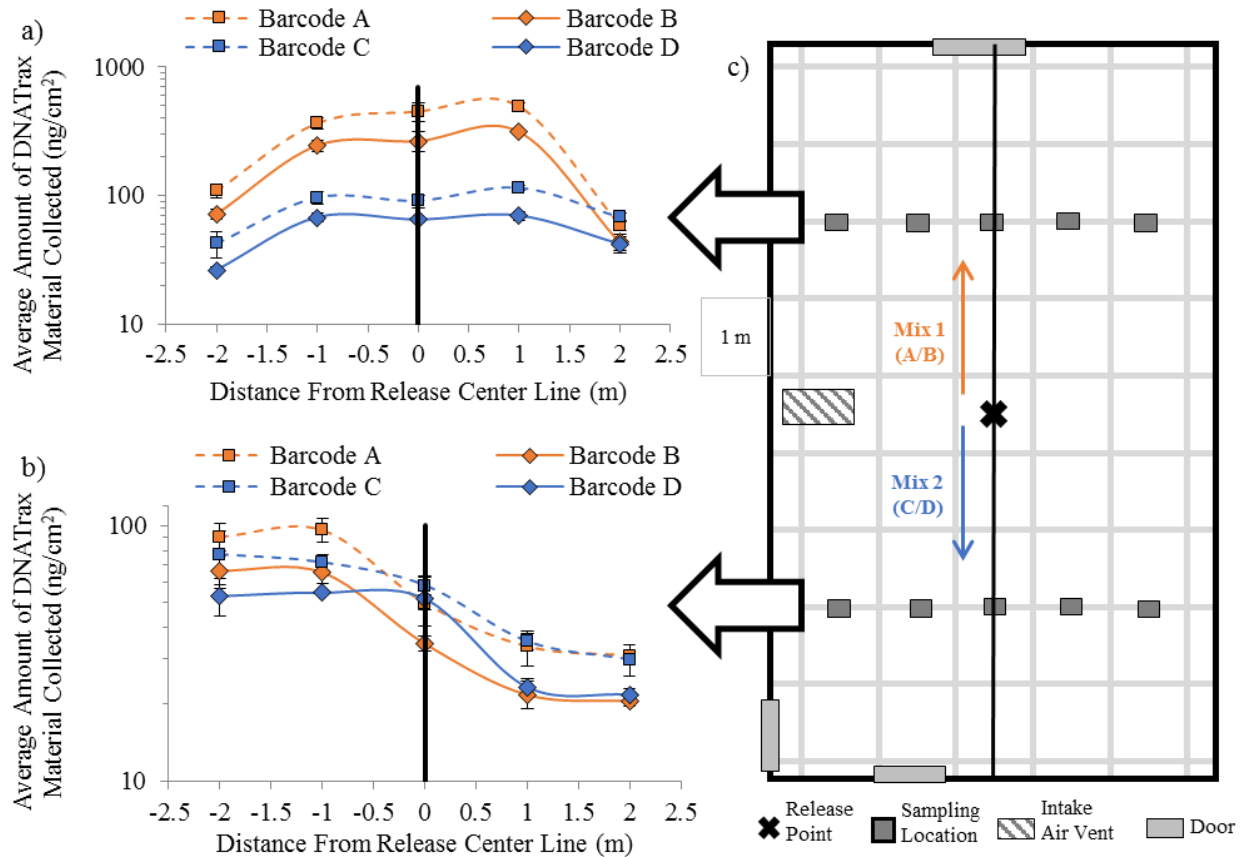


Figure 2.4 Average amount of DNATrax material collected on glass slides ($n=3$) along the cross-sections of the center line in a) the Mix 1 (A/B) direction and b) the Mix 2 (C/D) direction. Error bars indicate the standard deviation for the average amount collected on the glass slides. c) Schematic of testing location. Numerical values for each data point can be found in Table 2A.4.

The shape and relative relationships between of the deposition curves shown in Figure 2.4a represent the particle distribution expected for a room with no natural airflow. Barcodes A and B were released in the direction of these samplers, so there were more of Barcodes A and B collected than Barcodes C and D, which were released in the opposite direction. All four barcoded materials have nearly symmetrical distributions across the center line, also expected if there is no influence from the air flow. The Mix 2 direction (Figure 2.4b) has an asymmetry in

particle collection that was observed for all barcodes. While the exact source of the asymmetry is unclear, its presence across all barcodes adds confidence to the conclusion that this result accurately reflects the particle deposition in the room under normal, occupied conditions. The ability to simultaneously perform experiments in an occupied space with reproducible results is an advantageous characteristic of DNATrax that is clearly demonstrated within this experiment.

2.4 Conclusions

Accurate determination of the distribution of aerosol particles in an occupied space without disruption of the natural airflow in the room was accomplished using passive samplers in conjunction with DNATrax particles. Several passive sampling materials were compatible with the DNATrax simulant and subsequent PCR detection scheme. Using passive sampling, detection of DNATrax was achieved at both long distances up to 90 m from the release point and at shorter distances with 1-meter sampling resolution. Sampling reproducibility at the high resolution gave additional confidence in measurements of particle deposition at each location. Mixing together DNATrax powders with differing DNA barcodes before release provided two datasets experiencing identical experiment conditions from release through collection and detection. Using an additional pair of DNA barcodes, the effect of changing the initial direction of aerosol release was investigated. The combination of simultaneous DNATrax releases with passive sampling eliminates many of the underlying variables in aerosol transport studies including aerosolization efficiency, air flow fluctuations, sampling reproducibility and the impact of occupants in the test facility. By using simultaneous safe barcoded particles for aerosol test particles the environmental variability from experiment to experiment is eliminated.

APPENDIX

APPENDIX

DNA Template	Master Mix			
	Barcode A (359)	Barcode B (771)	Barcode C (431)	Barcode D (610)
Barcode A (359)	27.34±0.23	N/A	N/A	N/A
Barcode B (771)	N/A	28.97±0.07	N/A	N/A
Barcode C (431)	N/A	N/A	28.47±0.12	N/A
Barcode D (610)	N/A	N/A	N/A	29.01±0.14

Table 2A.1 Average cycle threshold for DNA templates used during the multiple barcode testing with each template’s master mix (1 fg DNA per reaction; n=3 reactions). Combinations in which the fluorescence did not exceed the threshold after 40 cycles are indicated by “N/A.”

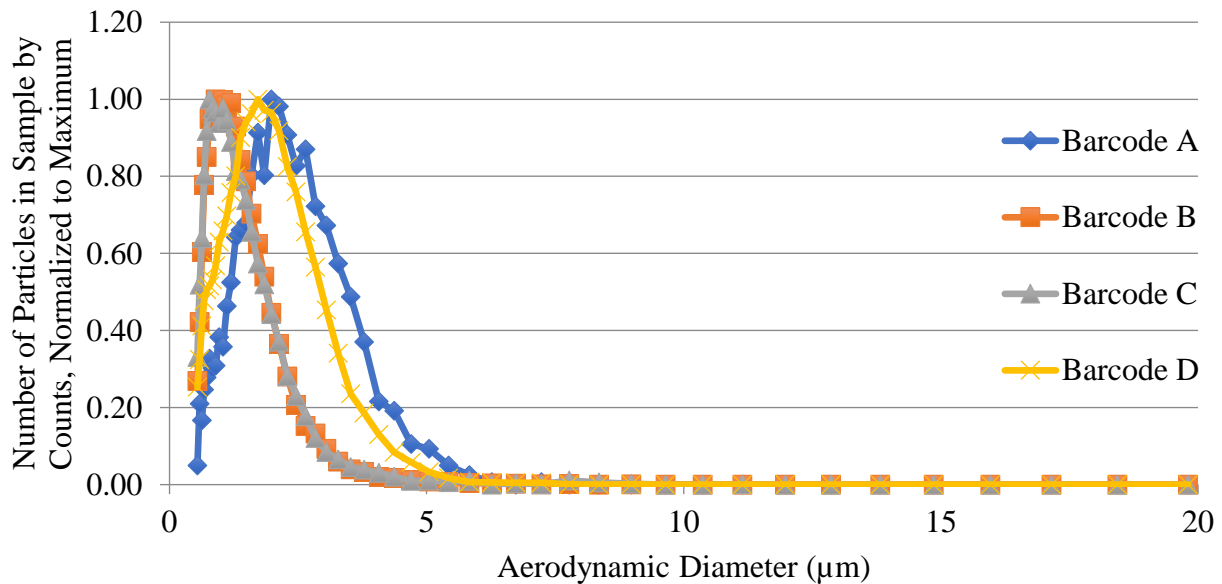


Figure 2A.1 Aerodynamic size distributions for DNATrax material of each label used during the multiple barcode testing.

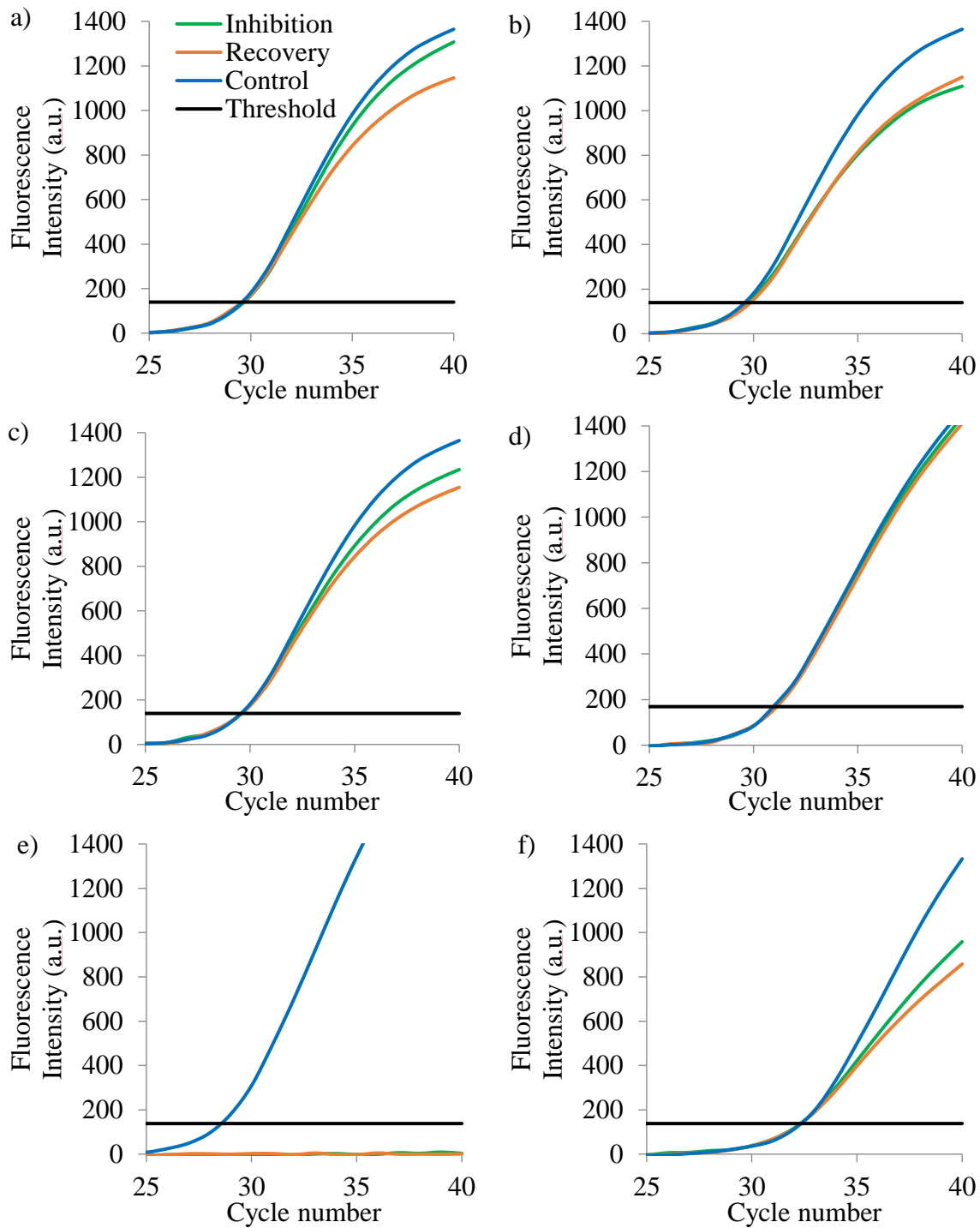


Figure 2A.2 PCR fluorescence curves for control (blue), inhibition (green), and recovery (orange) DNA solutions for the passive sampling materials a) polyester filter, b) glass slide, c) t-shirt cotton, d) filter paper, e) Post-It® note and f) Post-It® note with a 10x dilution. The threshold value is indicated by the black line.

Distance from Release (m)	Amount Collected on Post-It® Note (copies DNA/cm ²)	Amount Collected on Cotton T-shirt (copies DNA/cm ²)	Ratio of Amount Collected, (Post-It®/T-shirt)
3	1.19 ± 0.16 E+08	1.32 ± 0.41 E+08	0.90
9	4.68 ± 1.62 E+06	5.63 ± 0.68 E+06	0.83
27	3.10 ± 0.32 E+06	3.74 ± 0.77 E+06	0.83
60	1.61 ± 0.47 E+06	1.97 ± 0.11 E+06	0.82
63	2.71 ± 0.21 E+06	2.87 ± 0.31 E+06	0.94
72	2.28 ± 0.13 E+06	2.23 ± 0.14 E+06	1.02
90	3.66 ± 0.27 E+05	3.60 ± 0.21 E+05	1.02

Table 2A.2 Amount of DNATrax material collected on Post-It® notes and cotton t-shirt samplers (n=3; copies DNA/cm²) along a 90-m stretch of hallway.

Distance from Release (m)	Average amount collected (ng DNA/cm ²)	RSD
1	604.48	44.6%
2	496.52	12.4%
3	72.81	44.6%
4	13.63	26.9%
5	11.02	27.2%
6	11.20	36.7%
7	10.31	22.7%
8	9.98	33.7%
9	8.11	16.9%
10	14.26	40.8%

Table 2A.3 Average amount and relative standard deviation (RSD) of DNATrax material collected on Post-It® notes (n=3; ng/cm²) along at 1-m intervals during the second hallway testing.

Direction of Release	Distance from Release Line (m)	Barcode A (Mix 1)		Barcode B (Mix 1)		Barcode C (Mix 2)		Barcode D (Mix 2)	
		Avg.	St. Dev.						
Mix 1	-2	90.6	11.1	66.6	9.7	77.0	18.1	53.0	8.8
	-1	96.3	10.5	65.4	5.8	71.7	5.6	54.8	1.4
	0	49.7	3.0	34.5	2.3	58.3	4.9	51.8	11.1
	1	33.6	5.3	21.8	2.7	35.2	2.5	23.2	2.0
	2	30.9	1.0	20.6	1.0	29.9	4.2	21.7	1.3
Mix 2	-2	107.9	12.9	71.8	6.5	42.5	9.7	26.2	1.4
	-1	364.4	37.2	244.6	25.0	95.8	11.0	67.2	5.6
	0	448.5	75.9	264.6	46.4	90.5	10.3	64.6	2.6
	1	494.7	31.1	312.8	8.6	113.9	4.9	69.3	5.9
	2	58.8	5.5	43.5	6.2	67.8	5.4	41.9	6.2

Table 2A.4 Average amount of DNATrax material collected on glass slides (n=3; ng/cm²) along the cross-sections of the center line during the multiple barcode testing.

REFERENCES

REFERENCES

1. An Introduction to Indoor Air Quality. [EPA website]. March 16, 2016. <http://www2.epa.gov/indoor-air-quality-iaq/introduction-indoor-air-quality>. Accessed July 13, 2016.
2. Byron PR. Prediction of drug residence times in regions of the human respiratory tract following aerosol inhalation. *J Pharm Sci*. 1986. 75: 433–438.
3. Tsuda A, Henry FS, Butler JP. Particle transport and deposition: basic physics of particle kinetics. *Compr Physiol*. 2013. 3: 1437-1471.
4. Sinclair RG, Rose JB, Hashsham SA, Gerba CP, Haas CN. Criteria for selection of surrogates used to study the fate and control of pathogens in the environment. *Appl Environ Microbiol*. 2012. 78: 1969-1977.
5. Underwood DM, Herron DL, Croisant WJ. Whole-building dispersion of tracer gas after internal release in an administrative/classroom building. *ASHRAE Tran*. 2007. 113: 457-465.
6. Emanuel PA, Buckley PE, Sutton TA, Edmonds JM, Bailey AM, Rivers BA, Kim MH, Ginley WJ, Keiser CC, Doherty RW, Kragl FJ, Narayanan FE, Katoski SE, Paikoff S, Leppert SP, Strawbridge JB, VanReenen DR, Biberos SS, Moore D, Phillips DW, Mingioni LR, Melles O, Ondercin DG, Hirsh B, Bieschke KM, Harris CL, Omberg KM, Rastogi VK, Cuyk SV, Gibbons HS. Detection and tracking of a novel genetically tagged biological simulant in the environment. *Appl Environ Microb*. 2012. 78: 8281-8288.
7. King MF, Noakes CJ, Sleigh PA, Camargo-Valero MA. Bioaerosol deposition in single and two-bed hospital rooms: A numerical and experimental study. *Build Environ*. 2013. 59: 436-447.
8. Lopez-Andreo M, Lugo L, Garrido-Petierra A, Preto MI, Puyet A. Identification and quantitation of species in complex DNA mixtures by real-time polymerase chain reaction. *Anal Biochem*. 2005. 339: 73-82.
9. Harding RN, Hara CA, Hall SB, Vitalis EA, Thomas CB, Jones AD, Day JA, Tur-Rojas VR, Jorgensen T, Herchert E, Yoder R, Wheeler EK, Farquar GR. Unique DNA-barcoded aerosol test particles for studying aerosol transport. *Aerosol Sci Technol*. 2016. 50: 429-435.
10. Cable-Dunlap P, Trowbridge L, Bostick D, Lee D, Anderson B, Harter A, Kapsimalis R, Sexton L, De Gange J, Radford D. Comparison of active and passive environmental sampling for safeguards applications. *J Radioanal Nucl Chem*. 2013. 296: 943-949.

11. Sze To GN, Wan MP, Chao CYH, Fang L, Melikov A. Experimental study of dispersion and deposition of expiratory aerosols in aircraft cabins and impact on infectious disease Transmission. *Aerosol Sci Technol.* 2009. 43: 466-485.
12. Leith D, Sommerlatt D, Boundy MG. Passive sampler for PM_{10-2.5} aerosol. *J Air Waste Manage Assoc.* 2007. 57: 332-336.
13. Wagner J, Macher JM. Comparison of a passive aerosol sampler to size-selective pump samplers in indoor environments. *AIHA Journal.* 2003. 64: 630-639.
14. Ott DK, Kumar N, Peters TM. Passive sampling to capture spatial variability in PM_{10-2.5}. *Atmos Environ.* 2008. 42: 746-756.
15. Oldham MJ. Challenges in validating CFD-derived inhaled aerosol deposition predictions. *Inhal Toxicol.* 2006. 18: 781-786.
16. Tao Y, Inthavong K, Petersen P, Mohanarangam K, Yang W, Tu J. Experimental and CFD modelling of indoor air and wake flow from a moving manikin. *20th Australasian Fluid Mechanics Conference.* 2016.
17. Sajjadi H, Salmanzadeh M, Ahmadi G, Jafari S. Simulations of indoor airflow and particle dispersion and deposition by the lattice Boltzmann method using LES and RANS approaches. *Build Environ.* 2016. 102: 1-12.
18. Lu W, Howarth AT, Adams NM, Riffat SB. CFD modeling and measurement of aerosol particle distributions in ventilated multizone rooms. *ASHRAE Trans.* 1999. 105, part 2: 116-127.
19. Sohn MD, Apte MG, Sextro RG, Lai ACK. Predicting size-resolved particle behavior in multizone buildings. *Atmos Environ.* 2007. 41: 1473-1482.
20. Richmond-Bryant J, Eisner AD, Bixey LA, Wiener RW. Transport of airborne particles within a room. *Indoor Air.* 2006. 16: 48-55.
21. Udey, RN. Statistical data analyses of trace chemical, biochemical, and physical analytical signatures. *Doctoral dissertation.* 2013. Retrieved from MSU Libraries.

CHAPTER THREE: Stability of DNATrax Material as a Function of Exposure to UV Radiation

3.1 Introduction

Assessments of aerosol transport are facilitated by releases of tracer aerosols and quantitative measurements of particle numbers at various locations and times. The suitability of DNA-barcoded tracer aerosols (DNATrax) depends on stability of the DNA barcodes during the time between release and tracer measurement. Outdoor field studies that employ DNATrax present additional challenges not encountered with indoor particle releases including the potential for photodegradation of the DNA barcodes.

3.1.1 Photodegradation Mechanisms

Although DNA primarily absorbs UVC ($\lambda < 280$ nm) radiation, absorption by stratospheric ozone results in minimal solar energy below 290 nm reaching the earth's surface¹. With few solar UVC rays, the effects of UVB ($\lambda = 280-320$ nm) and UVA ($\lambda = 320-400$ nm) wavelengths must be considered in the photodegradation of DNA in outdoor environments. Direct absorption of a photon is more likely to occur with UVC or UVB radiation as the absorption of these wavelengths by DNA is more efficient than UVA². However, the presence of photosensitizers, or chromophores that become excited by the absorption of UVA photons, can lead to degradation reactions of the DNA³⁻⁴. Photosensitization is a common occurrence *in vivo* where chromophores such as riboflavin⁵ and benzophenone⁶ are present, but photosensitization can also play a role in isolated DNA degradation when other chromophores are present.

There are several mechanisms through which DNA photodegradation can occur including pyrimidine dimerization⁷⁻⁸ and purine oxidation⁵⁻⁶. Dimerization of adjacent pyrimidine bases

(thymine or cytosine) results in intra-strand crosslinking, while dimerization between pyrimidine bases on separate strands is termed inter-strand crosslinking. Intra-strand crosslinking of adjacent pyrimidines forms a range of photoproducts including 6,4-linked bases and cyclobutane dimers (Figure 3.1). Formation of cyclobutane dimers is favored over the 6,4-photoproduct because the 6,4-photoproducts require more extensive DNA unwinding and base rotations than the cyclobutane dimers⁹. Cyclobutane dimerization occurs with highest frequency between adjacent thymines¹⁰.

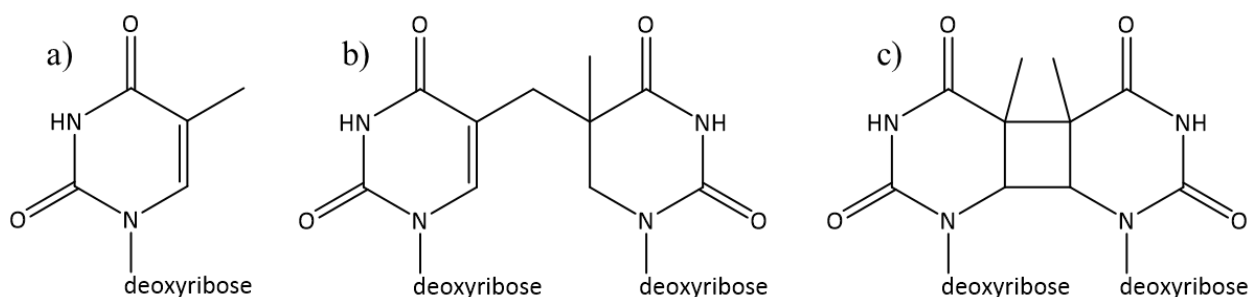


Figure 3.1 The pyrimidine base a) thymine and two products of photoinduced crosslinking of adjacent thymine monomers: b) 6,4-photoproduct and c) cyclobutane dimer.

Oxidation of guanine and the formation of 8-oxo-7,8-dihydroguanine (8-oxo-dGuo) occurs through two main types of reactions: Type I and Type II, summarized in Figure 3.2. In their simplest definitions, Type I reactions involve radical formation through electron transfer while Type II reactions involve energy transfer to oxygen¹¹. In Type I reactions, the electron transfer steps result in formation of a radical guanine, as guanine is the DNA base with the lowest ionization energy of DNA bases¹², followed by reaction of the guanine radical cation with oxygen to give the oxidized product (8-oxo-dGuo) (Figure 3.3a). While the final oxidation steps are the same, the radical guanine can be formed through either direct adsorption of UVC radiation which provides sufficient energy to ionize guanine (~ 7.8 eV; single photon of ~ 160

nm)¹²⁻¹³ or through reactions with radical reactive oxygen species (ROS), the product of electron transfer reactions between an activated photosensitizer and water. With little solar UVC radiation reaching the Earth's surface, Type I reactions that involve photosensitizers are more probable.

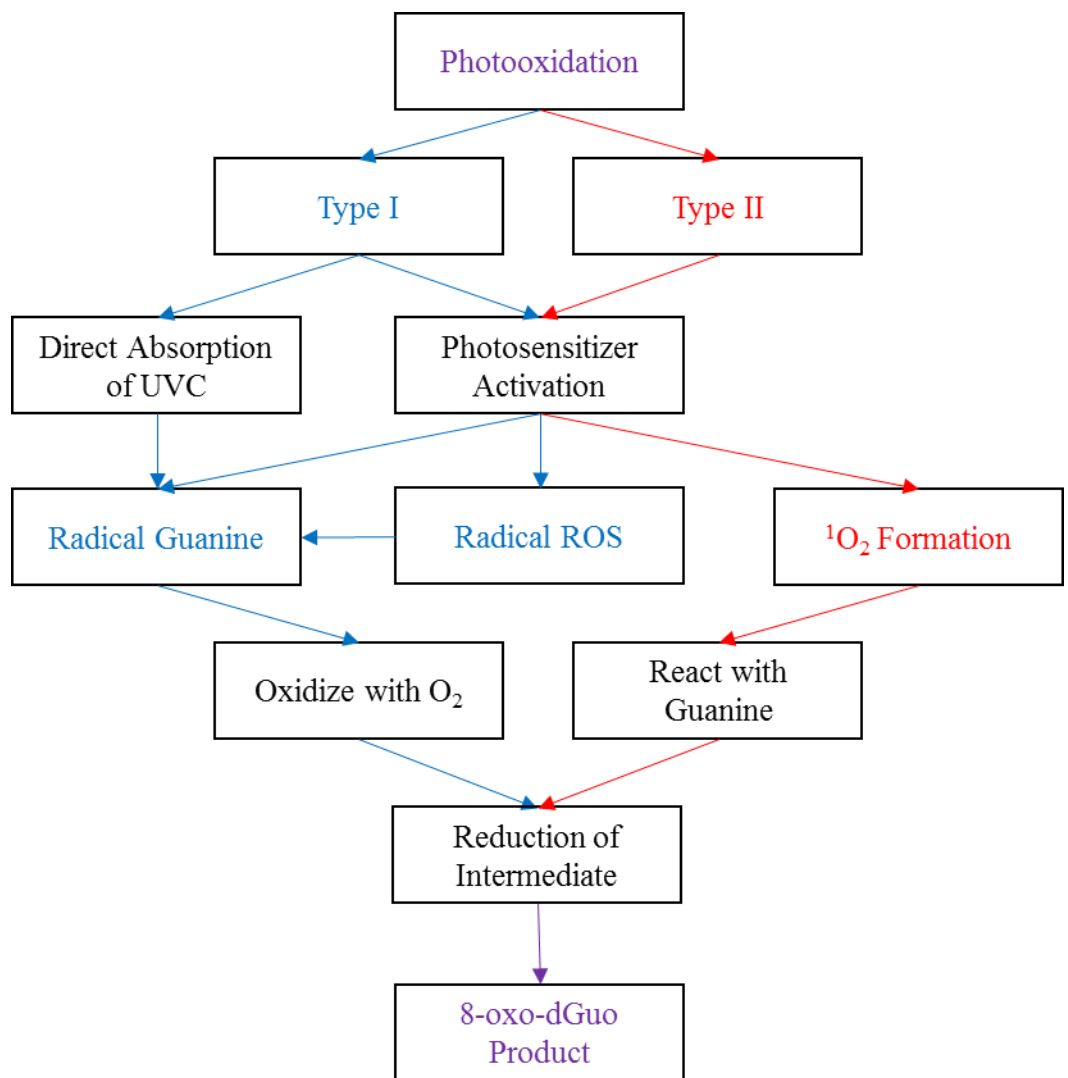


Figure 3.2 Summary of photooxidation reaction mechanisms.

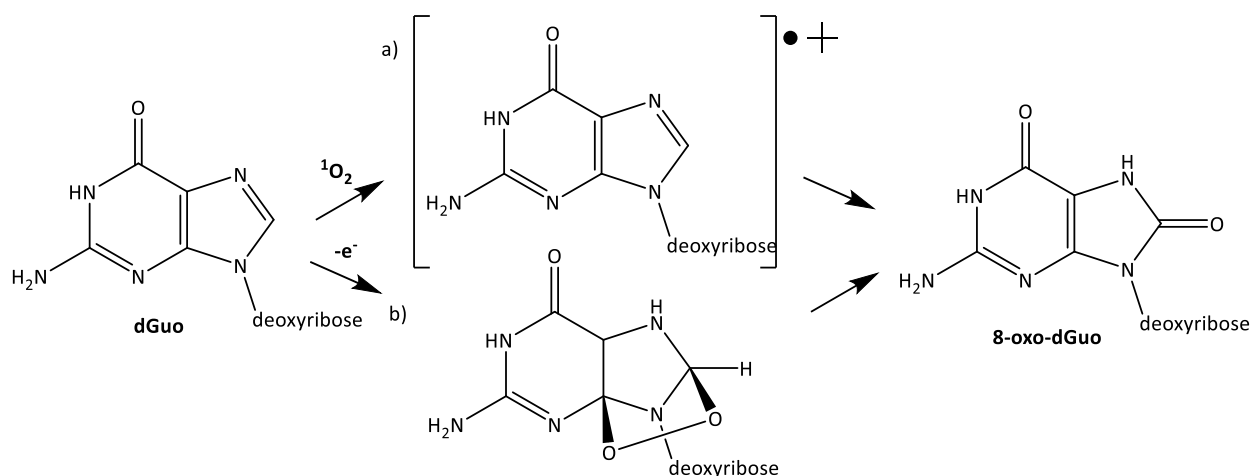


Figure 3.3 Formation of 8-oxo-7,8-dihydroguanine a) through ionization and reaction with water or oxygen and b) through reaction with singlet oxygen¹³.

Rather than transferring electrons, the activated photosensitizers in Type II reactions transfer energy to molecular oxygen to form singlet oxygen ($^1\text{O}_2$), another ROS. Upon energy transfer from photosensitizer excited state to molecular oxygen ground state, the spin of one of the unpaired electrons flips and the first singlet state, $^1\Sigma_g^+$, is formed^{5-6,14}. This singlet state relaxes to the second, lower energy, singlet state ($^1\Delta_g$) in which the electrons are spin paired¹⁵. In contrast to triplet oxygen ($^3\text{O}_2$) which has two half-filled π^* orbitals, the singlet state ($^1\text{O}_2$) has an empty orbital and acts as an electrophile, adding to the conjugated diene in guanine's imidazole ring (Figure 3.3b)¹⁶. Further reduction of this intermediate yields the 8-oxo-dGuo product¹⁷.

DNA lesions caused by both oxidation and dimerization interrupt DNA replication and inhibit the quantitative real-time polymerase chain reaction (qPCR) amplification used for DNATrax detection and quantitation¹⁸. qPCR analyses of UV-exposed biological material recommend amplifying DNA with short (100 bp or less) sequences to minimize the likelihood that amplified degradation products from nontarget DNA will interfere with measurement of the target sequence¹⁹. In this investigation, however, the entire length of the oligonucleotides used as

the DNA label in DNATrax is only ~100 bp in length, so any sites of degradation along the DNA sequence will result in a loss of amplification using the PCR assay. It is, therefore, important to understand the extent of this degradation with UV exposure to predict the decrease of detectable DNA label expected over the course of a release experiment performed outdoors.

3.1.2 Specific Aims

Outdoor releases of DNATrax aerosol tracer expose DNA to solar UV radiation. With quantification of the DNA vital to the detection of the tracer, degradation of the DNA that inhibits qPCR detection may compromise use of DNATrax in outdoor environments. Thus, the aim of this work is to determine the extent of DNA degradation that occurs with UV irradiation and assess whether steps might be taken to minimize photodegradation.

3.2 Materials and Methods

3.2.1 Material Production and DNA Analysis

Solid DNATrax material was produced via spray-drying using a Mini Spray Dryer B-290 (Büchi; Switzerland), using the parameters discussed in Chapter 2, Table 2.1²⁰⁻²¹. Several batches of solid material were produced with different DNA sequences, DNA concentrations, and concentrations of the UV-absorbing compound fluorescent brightener 220 (AK Scientific; Union City, CA), according to the concentrations in Table 3.2, preparations 1-5. Additionally, aqueous solutions containing DNA, organic food-grade tapioca maltodextrin (DE 10; Ciranda; Thailand), and fluorescent brightener 220 were prepared in PCR-grade water (Teknova; Hollister, CA) according to the concentrations in Table 3.2, preparations 6-8. Two different sequences of double-stranded DNA were used during these studies, denoted as Barcodes A and B, respectively

(see Table 3A.1. for sequence details). While the standard solutions of each DNA sequence used for calibration curves were purchased (Biosearch Technologies; Petaluma, CA), the stock solutions of DNA used for solid production and in the aqueous solutions listed in Table 3.1 were from standard DNA solutions previously amplified using a Taq-man quantitative real-time polymerase chain reaction (qPCR) assay (Invitrogen; Carlsbad, CA) with sequence-specific primers and probes (Integrated DNA Technologies; Coralville, IA). The components in the qPCR master mix and the thermal profile used for amplification are the same as those listed in Chapter 2, Tables 2.2a and 2.2b, respectively. These qPCR parameters were also used for quantification of DNA concentrations in the solid material and aqueous solutions before and after irradiation.

Prep	DNA Barcode	DNA Concentration (ng DNA/mg solids)	Maltodextrin Concentration (w/w)	Fluorescent Brightener 220 Concentration (w/w)
S1	A	12.5	99%	1%
S2	A	8.7	100%	N/A
S3	A	127.5	100%	N/A
S4	A	12.7	100%	N/A
S5	B	51.7	100%	N/A

Table 3.1 Composition of each solid material used for degradation experiments.

Prep	DNA Barcode	DNA Concentration (pg DNA/ μ L solution)	Maltodextrin Concentration in Solution (w/v)	Fluorescent Brightener 220 Concentration
A1	A	20.2	0.2%	0.002% (w/v); 1% (w/w) total solids
A2	A	20.4	0.2%	N/A
A3	B	21.4	3%	N/A

Table 3.2 Composition of each aqueous solution used for degradation experiments.

3.2.2 UV Degradation Under Germicidal Lamp

To assess the photodegradation of DNATrax, solid material and aqueous solutions containing DNA were irradiated using a germicidal lamp for up to 1 hour. The germicidal lamp used was a 15-watt lamp, delivering $136.8 \mu\text{W}\cdot\text{cm}^{-2}$ at 18 inches (46 cm) from the lamp (AirClean; Creedmoor, NC). This lamp generates significant emission in the UVC, UVA and visible ranges of wavelengths, and substantially less in the UVB wavelength range (Figure 3.4)²². While an imperfect simulator of solar irradiation, this lamp allows a consistent, known dose of each wavelength to be administered to the samples.

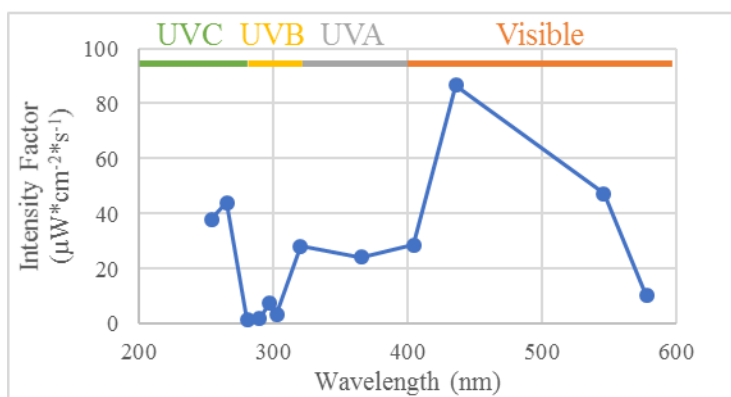


Figure 3.4 Intensity factors for light emitted across UV and visible wavelengths for the germicidal lamp used, as provided by the manufacturer.

For photoirradiation experiments, 10-20 mg of each solid material listed in Table 3.1 was weighed into uncapped glass scintillation vials that were placed 18 inches below the germicidal lamp and held at ambient temperature. Three vials of each material were set aside at the beginning of the experiment and 3 additional vials were removed from under the light at 5, 10, 30 and 60 minute time points. The solids were dissolved in Tris-EDTA buffer (Teknova; Hollister, CA) and further diluted for DNA quantification. For the aqueous solutions (Table 3.2),

50- μ L aliquots were prepared, placed in opened 2 mL polypropylene Eppendorf tubes, placed 35.5 cm directly below the lamp, and removed at appropriate time points (3 aliquots removed at each time point). The aqueous solutions were also diluted before DNA quantification so final concentrations would fall within the calibration curve concentrations. The amount of DNA in each sample was quantified by comparing the cycle threshold of each sample to a calibration curve of known DNA concentrations. Quantification of the extent of degradation was achieved by comparing the DNA concentration after each length of irradiation time with the control sample exposed to no irradiation.

3.2.3 Gel Electrophoresis Analysis

Formation of DNA degradation products was also assessed using gel electrophoresis (GE). GE analysis was performed using 20- μ L aliquots of dissolved solid material (Preps S3 and S4, Table 3.1) or aqueous solutions (Prep A2, Table 3.2). These aliquots were removed after irradiation and dissolution (in the case of the solids) but prior to dilution and PCR amplification. Aliquots were loaded onto a 4% agarose gel, pre-loaded with ethidium bromide stain, that provides 3.2 cm of run length for samples (Invitrogen; Carlsbad, CA). The electrophoretic separation was conducted for 15 minutes using the recommended program for the gel E-Base (Invitrogen; Carlsbad, CA). Images were visualized and recorded using a GeneFlash Bio Imaging UV transilluminator with an amber filter (Syngene; Frederick, MD). DNA length was determined by comparison to a 25-base pair (bp) DNA ladder (Invitrogen; Carlsbad, CA). Standard concentrations of the DNA sequence were also analyzed to ensure the solutions fell within the linear range of the GE analysis. Quantitation of band brightness was performed using ImageJ²³ and Microsoft Excel for Mac 2011 (Microsoft Corporation, Redmond, WA).

3.3 Results and Discussion

3.3.1 DNA Degradation Determination using qPCR

Quantification of DNA photodegradation by qPCR following irradiation showed exponential decay for both solid and aqueous samples (Figure 3.5). In all cases, the concentration of amplifiable DNA significantly decreased over the 60 minutes of light exposure (t-test, 95% confidence). While all irradiated samples showed evidence of degradation, the decrease in amplifiable DNA was most pronounced for the aqueous solutions, exhibiting a half-life of less than 10 minutes and yielding less than 3% of the DNA remaining intact after 60 minutes of irradiation. The addition of a UV absorber, fluorescent brightener 220, only provided minimal but statistically significant (t-test, 95% confidence) difference from solutions without the brightener at the 60-minute measurement, at which point the solutions containing the brightener underwent 0.62% more degradation than the solutions without it ($2.37 \pm 0.08\%$ of DNA remaining with brightener; $2.99 \pm 0.43\%$ of DNA remaining without brightener). Thus, the addition of the brightener did not protect the DNA in aqueous samples.

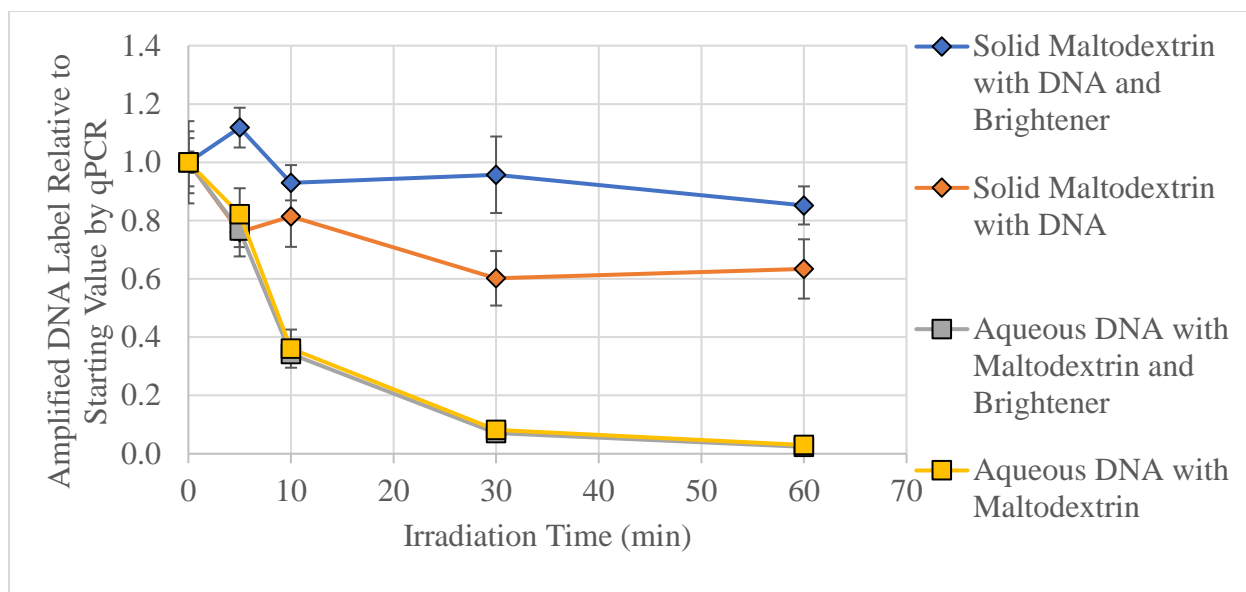


Figure 3.5 Average relative concentrations of DNA Barcode A sequence in solid DNATrax material and aqueous solutions both with and without Fluorescent Brightener 220 as a function of irradiation time, assessed using qPCR. Error bars indicate the standard deviation of three replicate samples irradiated simultaneously. Numerical values for this data is found in Table 3A.2.

When incorporated into the solid material, the DNA experienced less degradation than in aqueous solutions. After 10 minutes of irradiation, there was a significant difference between the degradation in the solid material ($93\pm 6\%$ and $79\pm 17\%$ DNA remaining with and without brightener, respectively) and that of the aqueous DNA ($34\pm 2\%$ and $36\pm 7\%$ DNA remaining with and without brightener, respectively). The brightener provided additional protection of the DNA in the solid samples, with a significant difference between the solid samples with and without brightener after 30 minutes of exposure (95% confidence), preserving at least 20% more DNA from degradation by its presence. Degradation in the solid samples occurred mainly during the first 10 minutes of exposure, with little further change in the amount of undegraded DNA

remaining after 30 and 60 minutes of exposure. This suggests that degradation mechanisms responsible for the DNA degradation over the first 10 minutes are inhibited at the later time points through either depletion of a reactant or generation of a photoprotective product that protects the DNA from photodegradation.

The shapes of the aqueous and solid DNA degradation curves provide information about the kinetics of the degradation reactions dominating in each material type. Direct absorption of UV radiation and its degradation via intramolecular thymine crosslinking is expected to proceed via first order kinetics, with reaction rates proportional to DNA concentration. The reaction rate of oxidative degradation depends on the formation of ROS more than the DNA concentration and can exhibit either zero-order kinetics when ROS concentration is in excess relative to the DNA, or higher order kinetics when the formation of ROS is slower than its reaction with DNA. To determine if the degradation proceeds via a first- or second-order reaction, the natural log of the concentration of amplifiable DNA and the inverse of the concentration were also graphed as a function of time for both the DNA in aqueous solution (Figure 3.6) and solid material (Figure 3.7). Both the first- and second-order plots give good linear correlation ($R^2 > 0.9$) for the aqueous solutions, although visual comparison reveals the data at irradiation times of 30 minutes or less are better fit by the first-order plot. This suggests that the rate-limiting step in the degradation process is the reaction between a ROS and the DNA. Each strand of DNA has multiple sites with the potential for oxidation or thymine cross-linkage, so multiple ROSs can interact with each strand. However, after only one site has been altered, the DNA will no longer replicate by qPCR and will be considered degraded. Thus, as the concentration of undegraded DNA decreases in the aqueous solution, the probability that the ROS will interact with an undegraded DNA strand also decreases, slowing the rate of reaction over time. The same first-order kinetics in effect in the

aqueous solution are not observed for degradation in the solid material, suggesting a more complex degradation mechanism. In the solid material, the extent of DNA degradation is not only limited by ROS formation and its reaction with undegraded DNA, but also by the mobility of reactive species within the solids to facilitate that reaction, and these processes may be slow. The degradation may also be inhibited by formation of photoproducts that either consume ROS or absorb UV light without leading to DNA degradation.

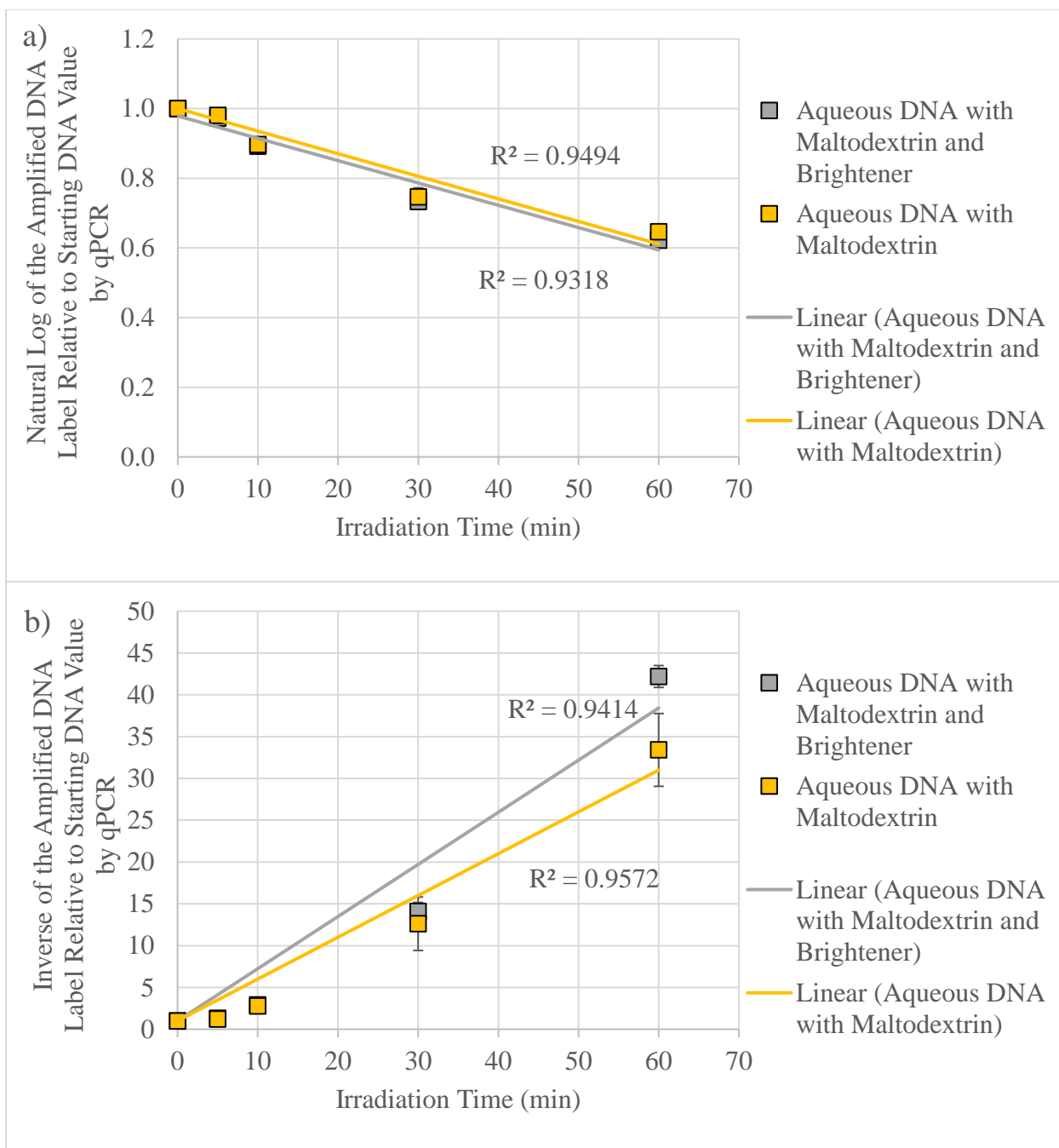


Figure 3.6 Ratio of the average a) natural log and b) inverse of the amplifiable DNA Barcode A sequence in aqueous solutions by qPCR after UV exposure to the amount of DNA present with no exposure. The error bars indicate the standard deviations of triplicate samples. The best fit lines for the data, forced through an intercept of 1, are also shown.

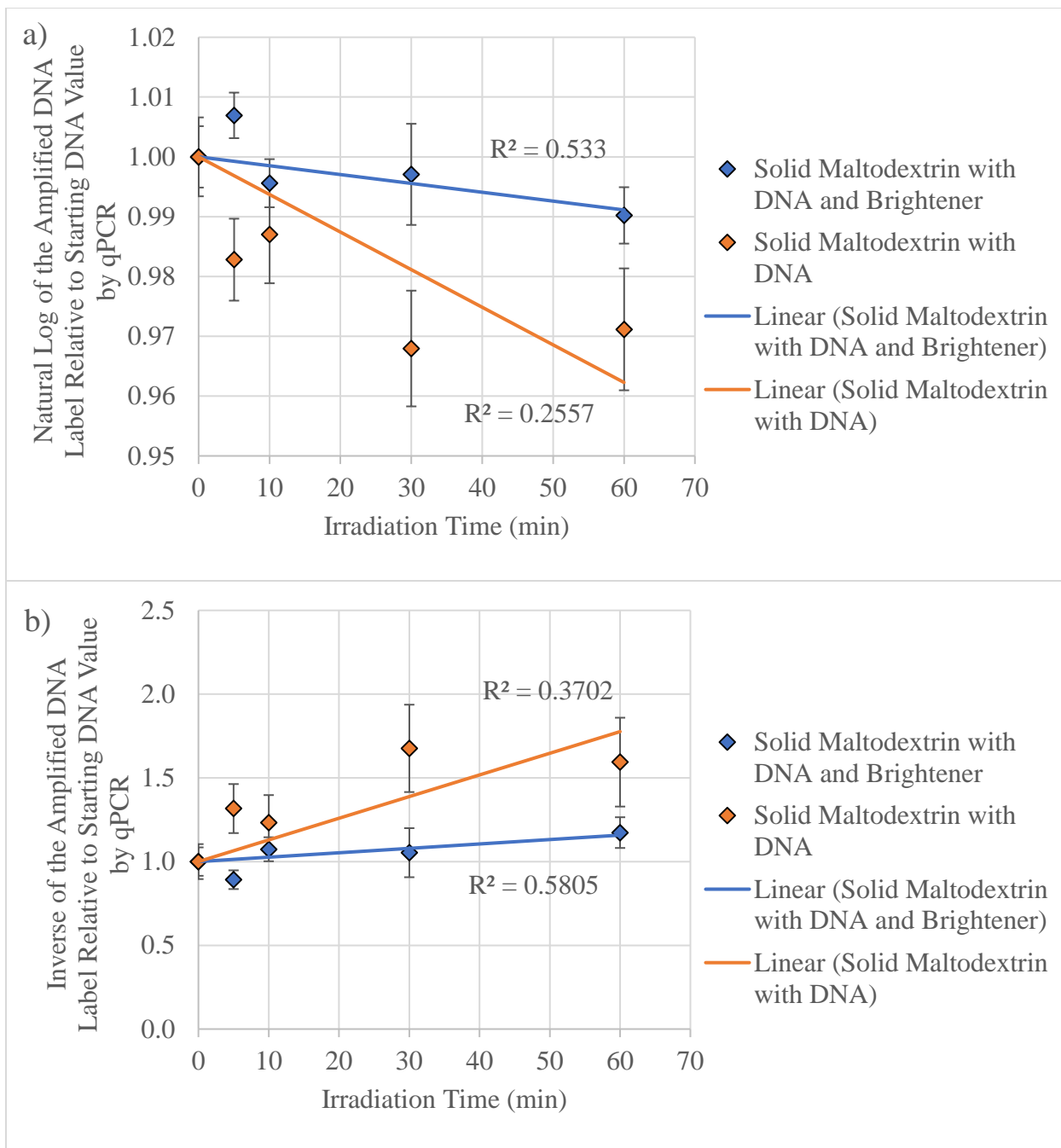


Figure 3.7 Ratio of the average a) natural log and b) inverse of the amplifiable DNA Barcode A sequence in solid material by qPCR after UV exposure to the amount of DNA present with no exposure. The error bars indicate the standard deviations of triplicate samples. The best fit lines for the data, forced through an intercept of 1, are also shown.

3.3.2 Degradation Products Analysis by Gel Electrophoresis (GE) and qPCR

Additional analyses, including gel electrophoresis and qPCR of a sequence with different guanine and thymine content, were performed to further evaluate degradation mechanisms dominating in each material type. Despite qPCR evidence for substantial photodegradation of DNA in aqueous solutions and somewhat less in solids, gel electrophoresis of products after irradiation showed minimal change in band migration or band brightness, with all of the major DNA bands present at approximately 100 bp (Figure 3.8a). However, visual assessment revealed a very weak band present in the “high” solid samples. After enhancement (Figure 3.8b), these low-intensity bands were shown to be at ~200 bp. Since DNA migrates as a function of size in GE, any changes in the migration of DNA or the presence of new bands would indicate that degradation has resulted in a change in the molecular size, either through chain fragmentation (shift to smaller size DNA) or inter-strand crosslinking that results in dimer formation (shift to larger size DNA). Given that the DNA of the low intensity band was roughly double the size of the DNA strand, this band suggests the formation of dimers within the “high” solid material. These dimer bands were not present after irradiation of either the aqueous or “low” solid material, indicating that either inter-strand crosslinking did not occur in these samples or the concentration of the dimers was below the limit of detection for GE analysis.

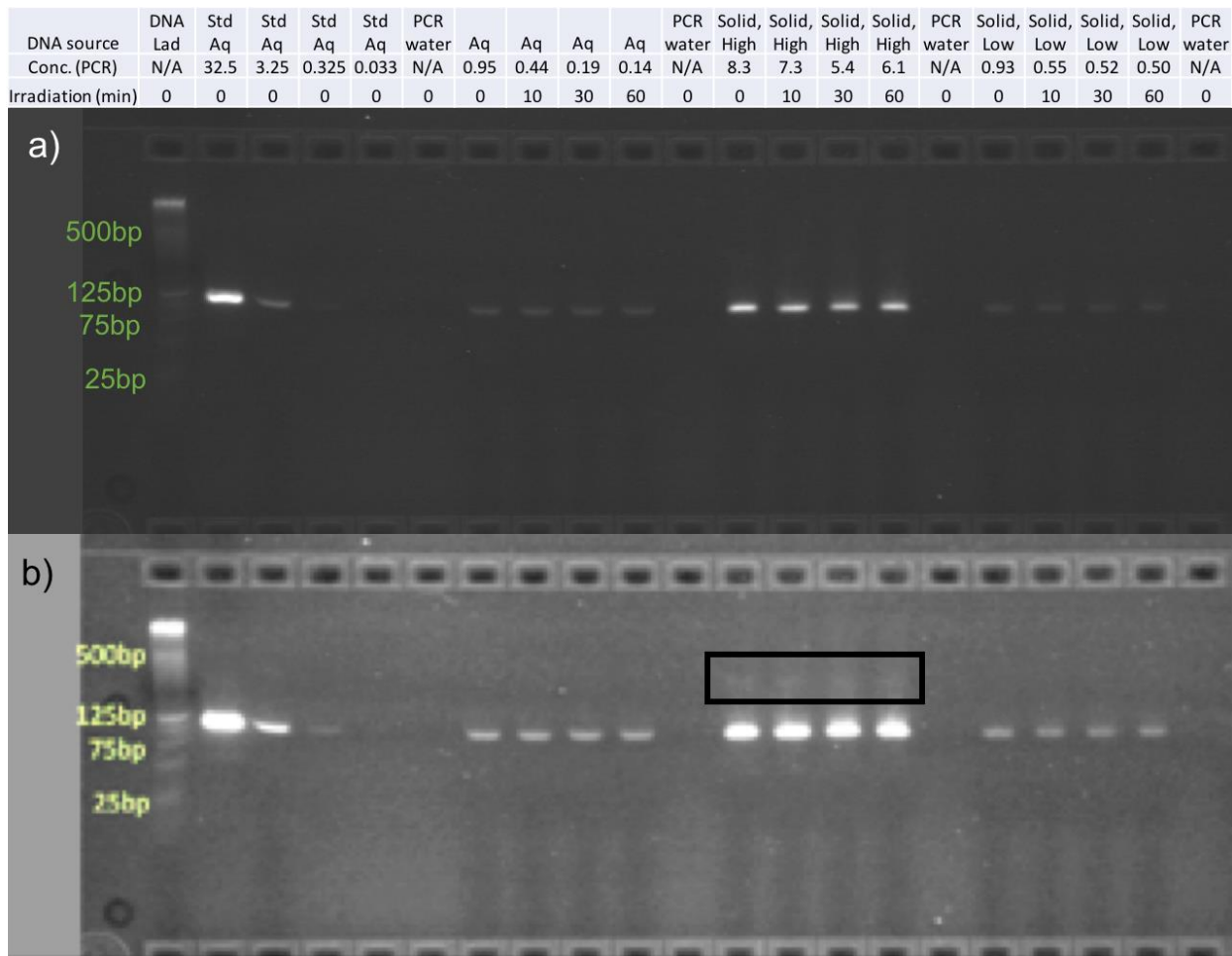


Figure 3.8 GE results of aqueous DNA (Aq) and solid material with DNA labeling (High and Low), after varying lengths of irradiation with no PCR amplification prior to GE analysis. Serial dilutions of a standard aqueous DNA solution (Std Aq) as well as a DNA ladder (DNA Lad) are included for reference. The image is shown both a) as acquired at the time of analysis and b) after adjustment of the brightness scale to improve visualization of low intensity bands, highlighted using the black box, using Adobe PhotoShop.

Direct comparison between the GE results and qPCR was achieved by quantifying the pixel brightness of the 100-bp band across each lane of the gel using ImageJ. These values were background subtracted using the pixel brightness for PCR water blanks and then plotted as a

function of migration distance. The results from each time point of the “high” solid material are shown as an example in Figure 3.9. Calculating the area under each curve and then dividing by the value of the “no UV” sample converts the pixel brightness into numerical values that can be compared to the qPCR values. This process was repeated for the aqueous DNA solutions and “low” solid material with the results of each shown in Figure 3.10a-c, respectively.

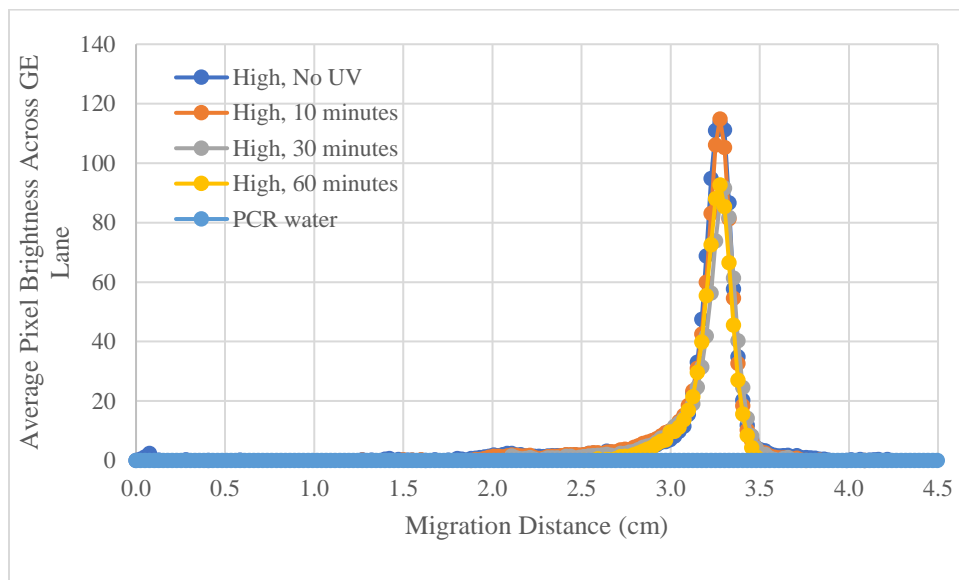


Figure 3.9 Average pixel brightness of horizontal pixels across a GE lane as a function of migration distance for UV-degraded samples of the Barcode A-labelled solid with high DNA labeling. All data have been background subtracted.

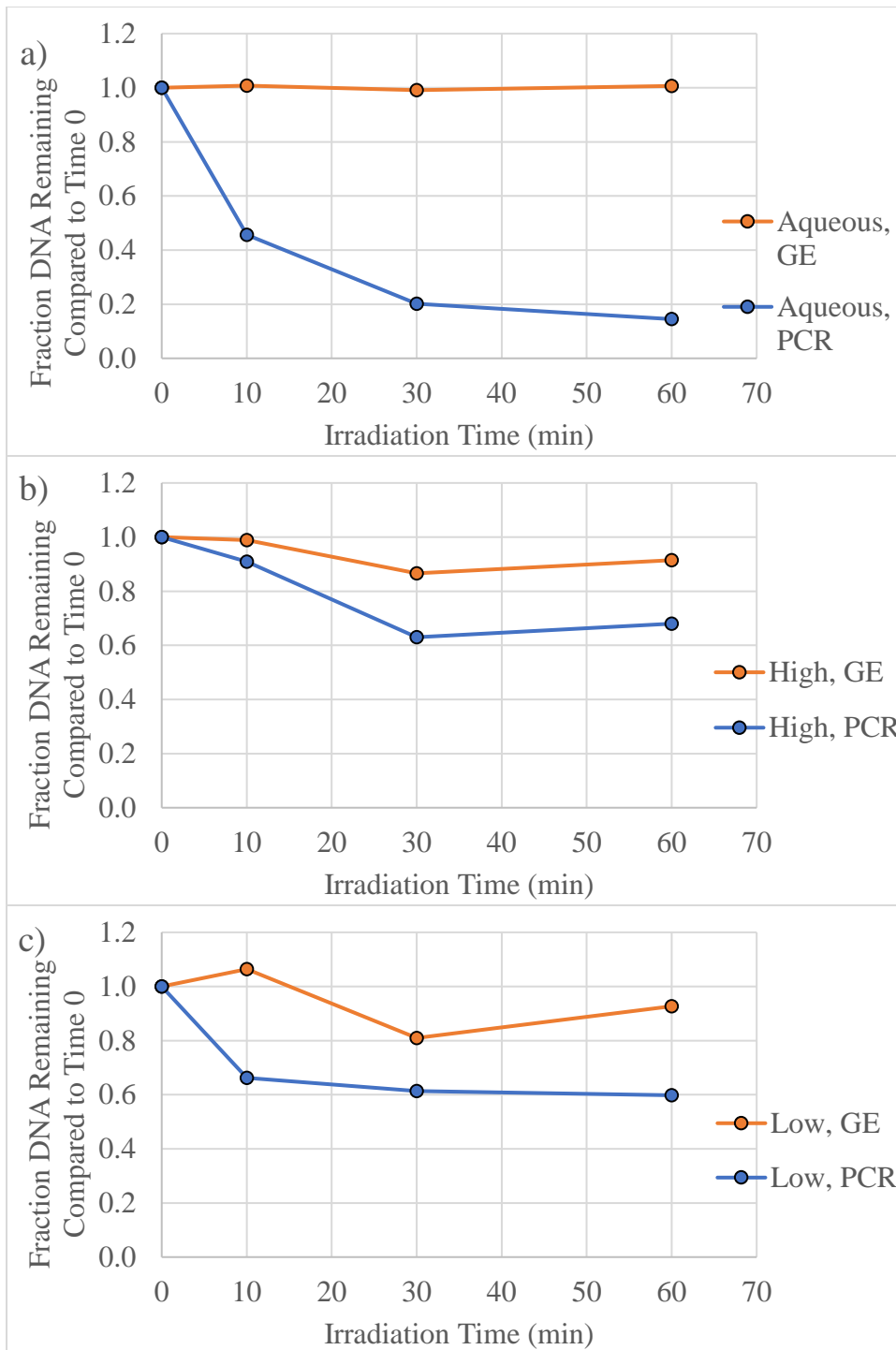


Figure 3.10 Fraction of DNA Barcode A sequence remaining quantified through qPCR as well as through GE with image brightness analysis for a) aqueous DNA, b) solid material with a high level of DNA labeling, and c) solid material with a low level of DNA labeling.

For all three sample types, the qPCR measurements reflect more extensive degradation than the changes in GE band intensity (Figure 3.10). This difference was most pronounced for the aqueous DNA solutions (Figure 3.10a). The aqueous solutions experienced no discernable change in GE band brightness, even after 60 minutes of irradiation while qPCR indicated 80% of the DNA was converted to unamplifiable forms. Thus the degradation mechanisms occurring in the aqueous samples result in no change in DNA length and occur through oxidation or intra-strand crosslinking. GE analyses did not yield evidence that lower molecular mass forms of DNA were produced during irradiation.

For the solid DNATrax particles, the results were more complex (Figure 3.10b and c). The GE results revealed that, at its steady state (measured by qPCR) at 30 minutes or more irradiation time, the 100-bp DNA concentration was reduced by 10-20% from the initial concentration. However, the qPCR results showed that the concentrations of amplifiable DNA had decreased by 30-40% from the initial concentration over the same time frame. Thus, only about half of the degradation that inhibited PCR also resulted in a change in the observed DNA size, so multiple degradation mechanisms must be present and yield more than one product. Based on the weak band seen with image enhancement indicating dimer formation (Figure 3.8b), the decrease the 100-bp band intensity corresponded to dimer formation due to inter-strand crosslinking. The remaining degradation assessed by qPCR that did not result in a size change is attributed to intra-strand crosslinking or oxidation similar to what was observed for the aqueous samples.

3.3.3 Degradation Mitigation

To determine if the extent of photodegradation is sequence-specific and thus favors mechanisms involving thymine or guanine, materials containing a second DNA sequence (Barcode B) were also irradiated under identical conditions. The original double-stranded DNA sequence, Barcode A, was 103-bp long with 58 thymine residues and 45 guanine residues between the two strands. Forty (69%) of these thymine residues were adjacent to another thymine residue and would provide a location for intra-strand crosslinking. The alternate double-stranded DNA sequence, Barcode B, was 100-bp long with a lower thymine content (48 thymine residues) and a higher guanine content (52 guanine residues). Twenty-six (54%) of the thymine residues in Barcode B were adjacent to another thymine.

Regardless of sequence, the aqueous and solid degradation curves resulted in similar behavior for the two sequences, with Barcode B DNA in the solid material again undergoing less extensive degradation than the aqueous DNA (Figure 3.11). However, using the Barcode B DNA sequence resulted in significantly less DNA degradation at each time point than when using the Barcode A DNA sequence for both aqueous DNA (77.7% vs. 3.0% DNA remaining after 60 minutes) and the solid material (93.2% vs. 63.4% DNA remaining after 60 minutes) (Figure 3.11; 95% confidence). While the similar curve shape suggests the same mechanisms dominate for both sequences, the lower thymine content and decreased extent of degradation in the 359 sequence is consistent with intra-strand crosslinking of adjacent thymines being a primary degradation mechanism. However, additional investigations using other sequences with varied thymine and guanine content are needed to establish principles useful for predicting rates of photodegradation.

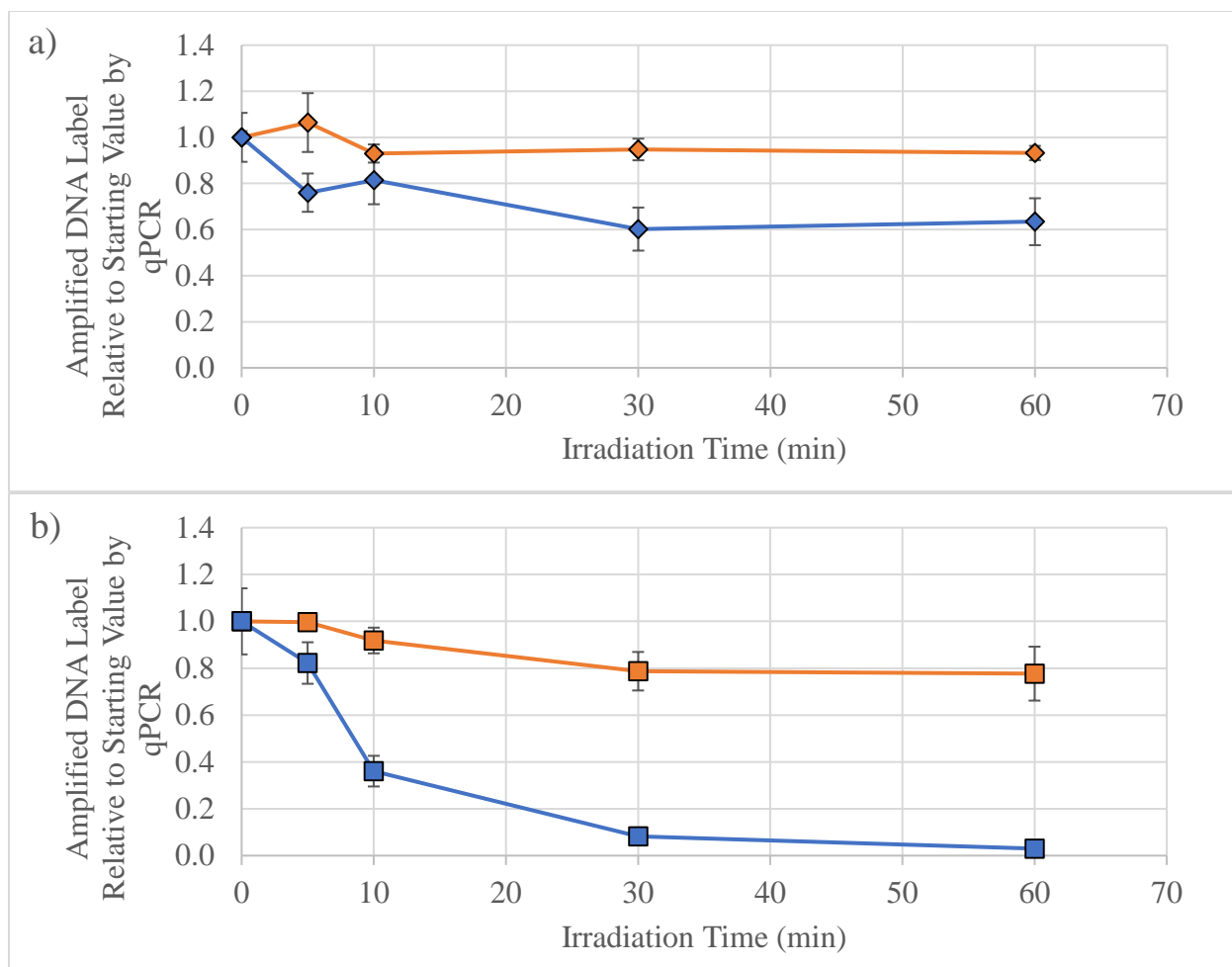


Figure 3.11 Average relative concentrations of either the Barcode A sequence (blue traces) or Barcode B sequence (orange traces) of DNA in a) solid DNATrax particles and b) aqueous solutions as a function of irradiation time, assessed using qPCR. Standard deviations are the three replicate samples irradiated simultaneously. Numerical data for these graphs can be found in Table 3A.3.

3.4 Conclusions

Irradiation of the original formulation of DNATrax (solid sample, maltodextrin, 610 sequence) yielded less than 40% loss in quantifiable DNA, even after 60 minutes of irradiation using a germicidal lamp that included wavelengths across the UVC, UVB, and UVA ranges. The

rate of degradation of the DNA barcode was more pronounced for aqueous samples of DNA than for the solid material, suggesting the solid matrix affords protection against UV-induced damage. The addition of a UV-absorber, Fluorescent Brightener 220, provided added protection for solid samples irradiated for 30 minutes or longer.

With a variety of wavelengths used for photodegradation, evidence of multiple degradation mechanisms was unsurprisingly observed. Comparison of qPCR and GE results revealed that the majority of degradation does not cause substantial change in DNA strand length, likely occurring through mechanisms such as intra-strand crosslinking or oxidation. While not present in aqueous samples, minor amounts of DNA dimers formed in the solid material through inter-strand crosslinking. The rate of degradation was qualitatively linked to the DNA sequence, although additional studies must be done to quantitatively correlate thymine or guanine content to the rate of reaction. While the use of a germicidal lamp provided control over some parameters associated with UV degradation, additional irradiation experiments that expose the DNA directly to sunlight should follow this work.

APPENDIX

APPENDIX

DNA Sequence Name	Length (bp)	AT Content	% T Adjacent to T	GC Content	Reverse Primer Length (bp)	Forward Primer Length (bp)	Probe Length (bp)
Barcode A	103	56% (116/206)	69% (40/58)	44%	20	20	31
Barcode B	100	48% (96/200)	54% (26/48)	52%	21	21	31

Table 3A.1 Base composition and length of the double-stranded DNA sequences used for DNATrax labeling and length of the primer and probe sequences.

Composition	Time	Solid		Aqueous	
		Average Concentration, Relative to Time 0	Standard Deviation	Average Concentration, Relative to Time 0	Standard Deviation
DNA, Maltodextrin, and Brightener	0	1.000	0.083	1.000	0.037
	5	1.119	0.068	0.766	0.057
	10	0.930	0.061	0.343	0.020
	30	0.957	0.131	0.071	0.005
	60	0.852	0.065	0.024	0.001
DNA and Maltodextrin	0	1.000	0.106	1.000	0.141
	5	0.760	0.083	0.822	0.089
	10	0.814	0.105	0.361	0.065
	30	0.602	0.093	0.082	0.023
	60	0.634	0.102	0.030	0.004

Table 3A.2 Average relative concentrations of Barcode A DNA in solid DNATrax particles and aqueous solutions both with and without Fluorescent Brightener 220 as a function of irradiation time, assessed using qPCR. Standard deviations are the three replicate samples irradiated simultaneously.

Composition	Time	Solid		Aqueous	
		Average Concentration, Relative to Time 0	Standard Deviation	Average Concentration, Relative to Time 0	Standard Deviation
DNA and Maltodextrin	0	1.000	0.027	1.000	0.009
	5	1.064	0.128	0.996	0.025
	10	0.930	0.039	0.918	0.055
	30	0.947	0.047	0.787	0.082
	60	0.932	0.031	0.777	0.115

Table 3A.3 Average relative concentrations of Barcode B DNA in solid DNATrax particles and aqueous solutions as a function of irradiation time, assessed using qPCR. Standard deviations are the three replicate samples irradiated simultaneously.

REFERENCES

REFERENCES

1. Gates DM. Spectral distribution of solar radiation at the Earth's surface. *Science*. 1966. 151: 523-529.
2. Mouret S, Philippe C, Gracia-Chantegrel J, Banyasz A, Karpati S, Markovitsi D, Douki T. UVA-induced cyclobutane pyrimidine dimers in DNA: a direct photochemical mechanism? *Org Biomol Chem*. 2010. 8: 1706–1711.
3. Foote CS. Type I and Type II mechanisms of photodynamic action. *ACS Symposium*. 1987. 339: 22–38.
4. Cadet J, Berger M, Decarroz C, Wagner JR, Van Lier JE, Ginot YM, Vigny P. Photosensitized reactions of nucleic acids. *Biochimie*. 1986. 68: 813-834.
5. Joshi PC, Gray TA, Keane TC. Protection of riboflavin and UVB sensitized degradation of DNA and RNA bases by natural antioxidants. *Ecotoxicol Environ Saf*. 2012. 78: 86–90.
6. Cuquerella MC, Lhiaubet-Vallet V, Cadet J, Miranda MA. Benzophenone photosensitized DNA damage. *Accounts Chem Res*. 2012. 45: 1558-1570.
7. Ballari RV, Martin A. Assessment of DNA degradation induced by thermal and UV radiation processing: Implications for quantification of genetically modified organisms. *Food Chem*. 2013. 141: 2130–2136.
8. Jenkins GJS, Parry JM. PCR-based methodology for the determination of the photoprotection afforded by sunscreen application. *Biotechniques*. 2000. 29: 1318-1320, 1323-1326.
9. Pfeifer GP. Formation and processing of UV photoproducts: effects of DNA sequence and chromatin environment. *Photochem Photobiol*. 1997. 65: 270-283.
10. Ravanat JL, Douki T, Cadet J. Direct and indirect effects of UV radiation on DNA and its components. *J Photoch Photobio B*. 2001. 63: 88-102.
11. Baptista MS, Cadet J, Mascio PD, Ghogare AA, Greer A, Hamblin MR, Lorente C, Nunez SC, Ribeiro MS, Thomas AH, Vignoni M, Yoshimura TM. Type I and Type II photosensitized oxidation reactions: guidelines and mechanistic pathways. *Photochem Photobiol*. 2017. DOI: 10.1111/php.12716.
12. Orlov VM, Smirnov AN, Varshavsky YM. Ionization potentials and electron-donor ability of nucleic acid bases and their analogues. *Tetrahedron Lett*. 1976. 48: 4377-4378.

13. Gomez-Mendoza M, Banyasz A, Douki T, Markovitsi D, Ravanat J-L. Direct oxidative damage of naked DNA generated upon absorption of UV radiation by nucleobases. *J Phys Chem Lett.* 2016. 7: 3945–3948.
14. Brash, DE. Sunlight and the onset of skin cancer. *Trends Genet.* 1997. 13: 410-414.
15. DeRosa MC, Crutchley RJ. Photosensitized singlet oxygen and its applications. *Coordin Chem Rev.* 2002. 233 234: 351 371.
16. Ravanat, JL, Cadet J. Reaction of singlet oxygen with 2'-deoxyguanosine DNA. Isolation and characterization of the main and oxidation products. *Chem Res Toxicol.* 1995. 8: 379-388.
17. Wei H, Cai Q, Rahn R, Zhang X. Singlet oxygen involvement in ultraviolet (254 nm) radiation-induced formation of 8-hydroxy-deoxyguanosine in DNA. *Free Radic Biol Med.* 1997. 23: 148-154.
18. Moore PD, Bose KK, Rabkin SD, Strauss BS. Sites of termination of *in vitro* DNA synthesis on ultraviolet- and N-acetylaminofluorene-treated ϕ X714 templates by prokaryotic and eukaryotic DNA polymerases. *Proc Natl Acad Sci.* 1981. 78: 110-114.
19. Ballari RV, Martin A. Assessment of DNA degradation induced by thermal and UV radiation processing: implications for quantification of genetically modified organisms. *Food Chem.* 2013. 141: 2130-2136.
20. Harding RN, Hara CA, Hall SB, Vitalis EA, Thomas CB, Jones AD, Day JA, Tur-Rojas VR, Jorgensen T, Herchert E, Yoder R, Wheeler EK, Farquar GR. Unique DNA-barcoded aerosol test particles for studying aerosol transport. *Aerosol Sci Technol.* 2016. 50: 429-435.
21. Udey, RN. Statistical data analyses of trace chemical, biochemical, and physical analytical signatures. *Doctoral dissertation.* 2013. Retrieved from MSU Libraries.
22. American Air & Water, Inc. Determining ultraviolet intensities using germicidal UV lamps. Received from AirClean Systems Service Technician on 4/9/17.
23. Rasband WS. ImageJ, U. S. National Institutes of Health, Bethesda, Maryland, USA, <https://imagej.nih.gov/ij/>, 1997-2016.

CHAPTER FOUR: Stability of DNATrax Material as a Function of Exposure to Humidity

4.1 Introduction

The suitability of DNA-barcoded tracer aerosols (DNATrax) as tracer aerosols for particle transport studies depends on the stability of both the particle's size and DNA barcode in the test environment. Outdoor field studies introduce conditions that can affect this stability that are otherwise controlled in indoor environments, including variable humidity levels. For example, in 2016 the relative humidity in East Lansing, MI, varied by an average of 37% within a single day with a difference between the highest and lowest humidities as high as 70% on June 29, 2016¹. With such a large change in relative humidity possible over the course of a single day, a better understanding of how this environmental change affects the particle size and DNA label is necessary. Both of these aspects are assessed within this Chapter.

4.1.1 Hygroscopicity of Sweeteners

Stability of a material under variable humidity depends in part on the material's hygroscopicity, or its affinity to absorb water. Hygroscopic materials will readily absorb the moisture present at high humidity environments and desorb water at low humidity. For a material made up of free-flowing particles, the absorption of water not only increases the particle mass but can also cause particle aggregation and a decrease in powder flowability^{2,3}. This is often a concern for the powdered food industries (*e.g.* spices, powdered milk) and is mitigated by the addition of bulking agents with low hygroscopicity such as maltodextrin, erythritol, xylitol and isomalt to the formulations⁴⁻⁶. The original DNATrax formulation utilizes maltodextrin as its

base material⁷, and other sweeteners may also serve as suitable materials. The chemical structures and select physical properties of these sweeteners are shown in Table 4.1.

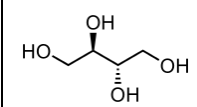
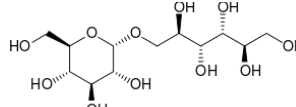
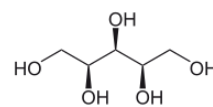
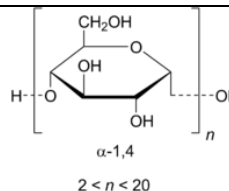
Compound	Erythritol ⁸	Isomalt ⁸	Xylitol ⁸	Maltodextrin ⁹
Melting Point (°C)	121	137	94	240
Glass Transition Temperature (°C)	-42	34	-22	138
Material Density (g/cm ³)	1.45	1.50	1.52	1.53
Critical Relative Humidity (%)	90%	85%	85%	>60%
Structure				

Table 4.1 Physical properties and chemical structure of commercially available sweeteners with low hygroscopicity.

While often expressed as a qualitative comparison (*e.g.* high or low), hygroscopicity can be more quantitatively compared using each material's sorption isotherms, which indicate the amount of water each absorbs as a function of water activity or relative humidity at a given temperature. From these isotherms, each sweetener's critical relative humidity, or relative humidity above which the moisture content rapidly increases with increasing humidity (a sharp increase in slope of the absorption), can be determined. While all four sweeteners are considered to be of low hygroscopicity, the value of this critical relative humidity and the extent of the material's moisture absorbance before the critical relative humidity varies. Erythritol and xylitol

are both sugar alcohols, with xylitol being more hygroscopic than erythritol. Erythritol absorbs less than 2% of its weight in water until the relative humidity exceeds 90%¹⁰⁻¹¹, while at 85% relative humidity xylitol absorbs nearly enough moisture to liquefy its crystals¹². Like erythritol, isomalt is stable across a range of humidities, but particularly absorbs moisture at relative humidities above 85%¹³.

Unlike the other sweeteners, which have well-defined physical properties, maltodextrin is a hydrolysis product of starch, so the oligosaccharide chain lengths and the corresponding physical properties in maltodextrin vary. Maltodextrins are described by their dextrose equivalent (DE) value, a measure of the extent of hydrolysis of the starch based on the presence of reducing sugar end groups, normalized to total mass⁹. The DE scale defines glucose as a value of 100, representing complete hydrolysis, and all other sweeteners relative to that value. Maltodextrins have a $DE < 20$ and their hygroscopicity increases as the DE increases, with the critical relative humidity at or above 60% RH^{3,14}. Below the critical relative humidity, maltodextrins can still absorb nearly 20% of their weight in water, with the exact value again depending on their DE¹⁵. With the absorption of water leading to particle aggregation, using a material with a higher critical relative humidity than maltodextrin that exhibits less water absorption prior to that point would reduce the probability of particle agglomeration and increase DNATrax's usefulness in humid environments.

4.1.2 Particle Size and Aerosol Transport

A main concern with moisture absorption by DNATrax is its potential to exert subsequent change on particle transport. The persistence of a particle as an aerosol is defined by its terminal settling velocity (V_{TS}), which in turn depends not only on the viscosity (η) of the gas

in which the particle is suspended and the gravitational constant (g), but also on the particle's density (ρ_p) and physical diameter (d_p) (Equation 4.1)¹⁶. If the density of the particle material increases due to water absorption or the effective diameter increases due to particle swelling or agglomeration, the settling velocity of the particle will also increase and the particle will settle at a faster rate than expected, altering the transport of the particle.

$$V_{TS} = \frac{\rho_p d_p^2 g}{18\eta}$$

Equation 4.1.

Since particle transport is linked to the physical diameter of an aerosol particle and defining that diameter is difficult for irregularly-shaped particles, an alternate metric of particle size is preferred: the aerodynamic diameter. The aerodynamic diameter (d_a) is defined as the diameter of a spherical particle of unit density (ρ_0 , 1 g/cm³) with the same settling velocity as the particle being measured (Equation 4.2). This allows for convenient comparison and prediction of the transport of particles of differing densities or shapes. The aerodynamic diameter can be expressed as a function of the physical diameter and density with a shape correction factor (X) that accounts for differences in resistive force as a function of shape (Equation 4.3). Since aerodynamic diameter is defined using spherical particles, the shape correction factor for spherical particles is 1.

$$d_a = \sqrt{\frac{18V_{TS}\eta}{g\rho_0}}$$

Equation 4.2

$$d_a = d_p \left(\frac{\rho_p}{\rho_0 X} \right)^{\frac{1}{2}}$$

Equation 4.3

The settling velocity and the corresponding aerodynamic diameter of a particle can be measured using the particle's time of flight in a controlled airflow¹⁷. In this work, aerodynamic diameter was measured using an Aerodynamic Particle Sizer Model 3321 (TSI; Shoreview, MN), which accelerates particles through a nozzle and into 2 partially overlapping laser beams¹⁸. The light scattered as the particle passes through the beams is focused onto a photodetector and recorded as a function of time. The overlapping beams result in a double-crested signal with the time between the peaks correlating to the particle's velocity and the aerodynamic diameter, with larger particles requiring more time to travel between the beams than smaller particles. The aerodynamic diameters recorded are binned into 23 bins spanning ~20 μm in diameter.

For particles of a broad size distribution binned into discrete values, the aerodynamic diameter is reported using the mass median aerodynamic diameter (MMAD) and the 90th mass percentile (d90). The calculation of these values is summarized in Figure 4.1. The size distribution is converted from the number of particles of each size initially reported to the fraction of the mass of material represented by the counts of each size. The particle diameter at which half of the mass is distributed across smaller diameters and half across larger diameters is the mass median aerodynamic diameter. The 90th percentile of this distribution is the d90. The combination of MMAD and d90 indicate the center and width of the mass distribution.

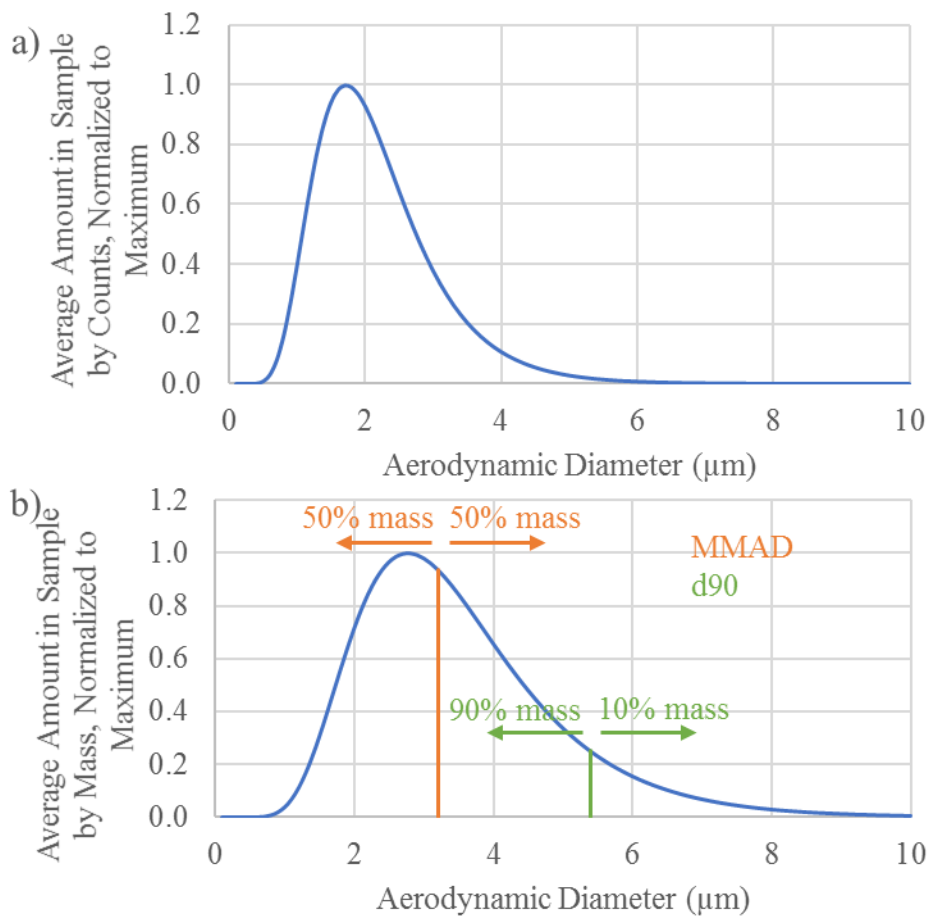


Figure 4.1 Example of a lognormal distribution of particle size plotted a) by the fraction of the total number of sample counts at each aerodynamic diameter and b) by the fraction of the total mass of particles represented by particles of each aerodynamic diameter. The mass median aerodynamic diameter (MMAD) and 90th mass percentile (d90) are marked in panel b.

4.1.3 DNA Degradation Mechanisms

In addition to size stability, the DNA label also needs to be stable with exposure to variable humidities to be useful in outdoor environments. While the presence of moisture in the particle is not detrimental to DNA by itself¹⁹, it does facilitate the formation of reactive oxygen species and subsequent oxidation of guanine residues in the presence of UV radiation²⁰. A more

detailed discussion of oxidative degradation can be found in Section 3.1.1 of this dissertation. In addition to the oxidative mechanisms, degradation could also occur through contamination by deoxyribonuclease (DNase) enzymes, which hydrolytically cleave the phosphodiester linkages of the DNA backbone. In the case of both degradation mechanisms, the resulting DNA might no longer be amplified and detected using quantitative real-time polymerase chain reaction (qPCR), offering potential loss of particle detection sensitivity under these conditions. Therefore, it is important to determine the extent to which the DNA is affected by humid environments.

4.1.4 Specific Aims

With potential for water absorption or desorption by DNATrax particles under variable humidities, the stability of the particle size and DNA label is uncertain. To assess the stability of both the aerodynamic diameter and the DNA label, the size and DNA label of DNATrax material was monitored over time with exposure to high, low, and cycling humidities. Particle production and hygroscopic stability of additional bulk materials were also performed to investigate the DNATrax formulation for environments with variable humidities.

4.2 Materials and Methods

4.2.1 Solid Material Production Conditions

Four food-grade sweeteners were selected as potential bulk material for DNATrax: xylitol (NOW Foods; Bloomingdale, IL), isomalt (Confectionery Arts International; New Britain, CT), erythritol (NOW Foods; Bloomingdale, IL), and maltodextrin (DE 10; Ciranda; Thailand). Aqueous solutions of each were prepared in PCR-grade water (Teknova; Hollister, CA) and spray-dried using a Mini Spray Dryer B-290 (Büchi; Switzerland), according to the

parameters previously listed in Table 2.1^{7,21}. Of these sweeteners, only erythritol and maltodextrin produced the free-flowing powder necessary for the particles to be used as an aerosol simulant (see Section 4.3.1 for discussion) and particles were made using each of these sweeteners both with and without DNA labeling. For the DNA label, standard solutions of a custom double-stranded DNA sequence were purchased (Biosearch Technologies; Petaluma, CA) and used for calibration curves. The stock solutions of DNA used for solids production were standard DNA solutions amplified using a Taq-man quantitative real-time polymerase chain reaction (qPCR) assay (Invitrogen; Carlsbad, CA) with sequence-specific primers and probes (Integrated DNA Technologies; Coralville, IA). The components of the qPCR master mix and the thermal profile used for amplification and quantitation are identical to those listed in Tables 2.2a and b, respectively. These qPCR parameters were also used for quantitation of the DNA labeling in the material, using approximately 20 mg (exact mass known) of solid material dissolved in Tris-EDTA buffer (Teknova; Hollister, CA) and diluted before qPCR analysis. Each sample was analyzed with triplicate instrumental replicates at two different dilution factors (1:10⁴ and 1:10⁵). The level of DNA in each solution was determined using a calibration curve of standard concentrations and the labeling levels in solid materials are reported as the copies of DNA per particle of 2- μ m aerodynamic diameter.

4.2.2 Particle Size Determination

The aerodynamic diameter of the material was determined by first aerosolizing material into a closed 5-gallon (18.9 L) chamber using an eductor (MIT Lincoln Laboratory; Lexington, MA) with a compressed gas source (Falcon Safety Products; Branchburg, NJ) (Figure 4.2). Aerosolization took place over a period of 2-3 seconds. Air was drawn out of the chamber by an

Aerodynamic Particle Sizer (APS) Model 3321 (TSI; Shoreview, MN) at a rate of 1 L/min and was sampled for 30 seconds immediately after aerosolization. These data were exported from the APS software (TSI; Shoreview, MN) and further calculation of the distribution's MMAD and d90 were performed in Microsoft Excel for Mac 2011 (Microsoft Corporation, Redmond, WA).

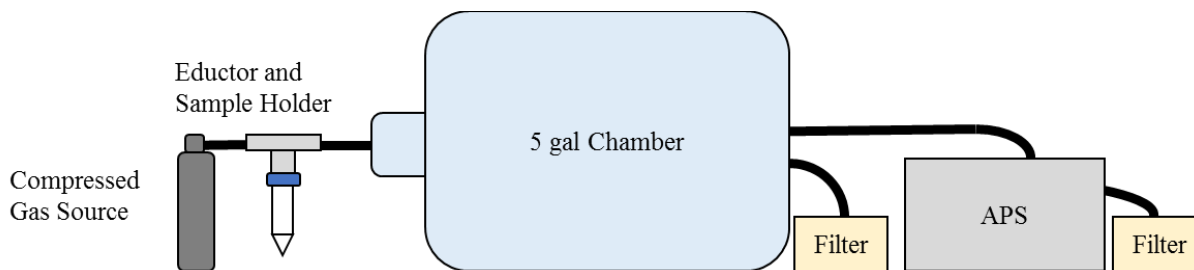


Figure 4.2 Diagram of the aerosol generation and sizing method used.

4.2.3 Humidity Chamber Set-up

Humidity chambers were used to maintain a constant relative humidity for sample incubation. The chambers consisted of airtight containers (Rubbermaid; Atlanta, GA) measuring 22.9 cm x 22.9 cm x 7.6 cm and were stored in an oven set to 25°C. Each chamber contained a 30-mL beaker holding a saturated salt solution of either sodium chloride (high humidity chamber) (Sigma Aldrich; St. Louis, MO) or lithium chloride (low humidity chamber) (Sigma Aldrich; St. Louis, MO). Saturated salt solutions have defined vapor pressures which control the humidity within a closed chamber, with predicted relative humidities of 75.8% and 12.0% at 25°C for the high and low humidity chambers, respectively²². The conditions within the chamber were monitored using an RHT20 Humidity and Temperature Datalogger (Extech; Waltham, MA), which recorded both the temperature and relative humidity in the chamber every 1 minute for the duration of the experiment. An additional datalogger was placed on the benchtop to

monitor the temperature and humidity of the ambient lab air. After the experiment was completed, the recorded data were exported from the manufacturer's software and plotted using Microsoft Excel for Mac 2011.

4.2.4 Humidity Chamber Incubation

To study the effects of humidity on particle size, ~100 mg of unlabeled (no DNA) maltodextrin or erythritol material were weighed into scintillation vials. Three aliquots of each material were placed, uncapped, in the high humidity chamber; 3 were placed in the low humidity chamber; and 3 on the benchtop (ambient). An additional 3 aliquots of each material were rotated between the high and low humidity chambers according to the schedule in Table 4.4 to mimic the fluctuations in humidity encountered in outdoor environments. At each time point (Day 0, 1, 2, 5, and 8), each sample was removed from the chamber, capped, weighed, sized according the method described in Section 4.2.2, reweighed, and placed into the appropriate chamber. While Radosta³ *et al.* reported maltodextrin (DE4) reaching equilibrium in 3-6 days at 98% relative humidity, the humidity of an outdoor environment fluctuates throughout a single day and these incubation times represent a middle ground between the two time scales.

Time Into Chamber	Time Out of Chamber	Incubation Time	Rotation	High	Low	Ambient
Day 0	Day 1	1 Day	12% RH (Theor.)	76% RH (Theor.)	12% RH (Theor.)	Benchtop
Day 1	Day 2	1 Day	76% RH (Theor.)	76% RH (Theor.)	12% RH (Theor.)	Benchtop
Day 2	Day 5	3 Days	12% RH (Theor.)	76% RH (Theor.)	12% RH (Theor.)	Benchtop
Day 5	Day 8	3 Days	76% RH (Theor.)	76% RH (Theor.)	12% RH (Theor.)	Benchtop

Table 4.2 Incubation location for the rotation, high, low, and ambient aliquots during the hygroscopicity study.

To determine the effect of humidity on the DNA label, ~20 mg aliquots of labeled maltodextrin or erythritol material were weighed into scintillation vials. Similar to the non-labeled material study described above, triplicate aliquots were prepared as high, low, ambient, and rotation aliquots and incubated according to the schedule in Table 4.2. Three additional aliquots of each labeled material were prepared and the DNA content was determined using the qPCR method described in Section 4.2.1. At Day 8 of the experiment, the DNA in all incubated aliquots was also quantified using qPCR.

4.3 Results and Discussion

4.3.1 Particle Production using Alternative Sweeteners

Of the four sweeteners – maltodextrin, erythritol, xylitol, and isomalt – only maltodextrin and erythritol produced particles suitable for use as an aerosol tracer. Production with xylitol did not yield solid material, but rather produced a viscous sticky liquid. The melting point of xylitol (94°C) is below the spray dryer’s outlet temperature (110°C) and the solid material produced melted as it was collected. Reducing the outlet temperature to below 94°C required reducing the

overall temperature of the drying gas, which resulted in incomplete drying of the solids and still no particle formation. Given this, no further testing was performed using xylitol. While the melting point of isomalt (137°C) is above the outlet temperature and a solid material formed, the solid was a rubbery texture rather than a free-flowing, crystalline solid. This is due to the production temperature being above the glass transition temperature (34°C), or the temperature at which an amorphous solid changes from a hard and brittle “glassy” state at temperatures below this point to a viscous or rubbery state with at temperatures above this point²³. Once cooled to below the glass transition temperature, the rubbery state will relax into a crystalline solid. However, the solid formed is not a free-flowing powder, a necessary characteristic for use as an aerosol tracer. Erythritol and maltodextrin both produced solids as free-flowing powders. Production with erythritol gave a much lower percent yield than maltodextrin (~5% vs. ~50%) as much of the erythritol material was accumulated as a sticky coating on the walls of the spray dryer due to its lower melting point and glass transition temperature. However, free-flowing material made of each of these sweeteners was used in further studies.

4.3.2 Effect of Humidity Exposure on Bulk Weight

The changes in weight of the maltodextrin-based material with time in each chamber reflect maltodextrin’s hygroscopic nature (Figure 4.3a). When stored continuously in the high humidity chamber (62.8 ±2.2% relative humidity), the weight of the maltodextrin material increased by 3.0% after 1 day in the chamber and did not significantly change for 7 days afterward (t-test; 95% confidence), having reached equilibrium within the first day. Radosta³ *et al.* reported maltodextrin (DE 4) increased in weight by ~10% per day until it reached equilibrium under 98% humidity. While the humidity in this chamber is lower than in their

study, the 3% increase is well below this upper limit for the maximum amount of water absorbed within a day and it is reasonable that the material can reach equilibrium in this time scale. When stored in the low humidity chamber ($19.4 \pm 3.7\%$ relative humidity), the weight of the maltodextrin-based material continually decreased by at least 0.5% of the bulk weight at each time point over the 8 days of the experiment (95% confidence), consistent with moisture being present in the material at the beginning of the experiment. A total of 5.5% of the bulk weight was lost by the low-humidity aliquots over the 8 days of the experiment with no weight equilibrium reached in that time. The lack of weight equilibrium with the low-humidity incubation is likely an effect of the gradual decrease in RH in the low humidity chamber over the course of the experiment. The humidity level in the low humidity chamber gradually decreased from 23.7% RH just before the samples were removed from the chamber on Day 1 to 14.4% RH just before sample removal on Day 8. As the saturated lithium chloride solution absorbs water over time to reduce the humidity level, the concentration of the dissolved salt at the surface of the slurry is decreased compared to the bulk solution. With the humidity controlled by the vapor pressure of the solution (related to the salt concentration), this dilution over time would limit the effectiveness of the lithium chloride solution at reducing the humidity in the chamber and prevent the humidity chamber from reaching its literature value for humidity. The solution was stirred at each time point, increasing the salt concentration at the surface and allowing more water to be absorbed, effectively lowering the relative humidity in the chamber with cycle of stirring and humidity equilibration. In future experiments, the salt slurry should be continuously stirred or have a higher ratio of slurry surface area to chamber volume to bring the chamber humidity to match the literature values. The change in sample weight has a strong positive correlation with this humidity change (R-squared value of 0.8700).

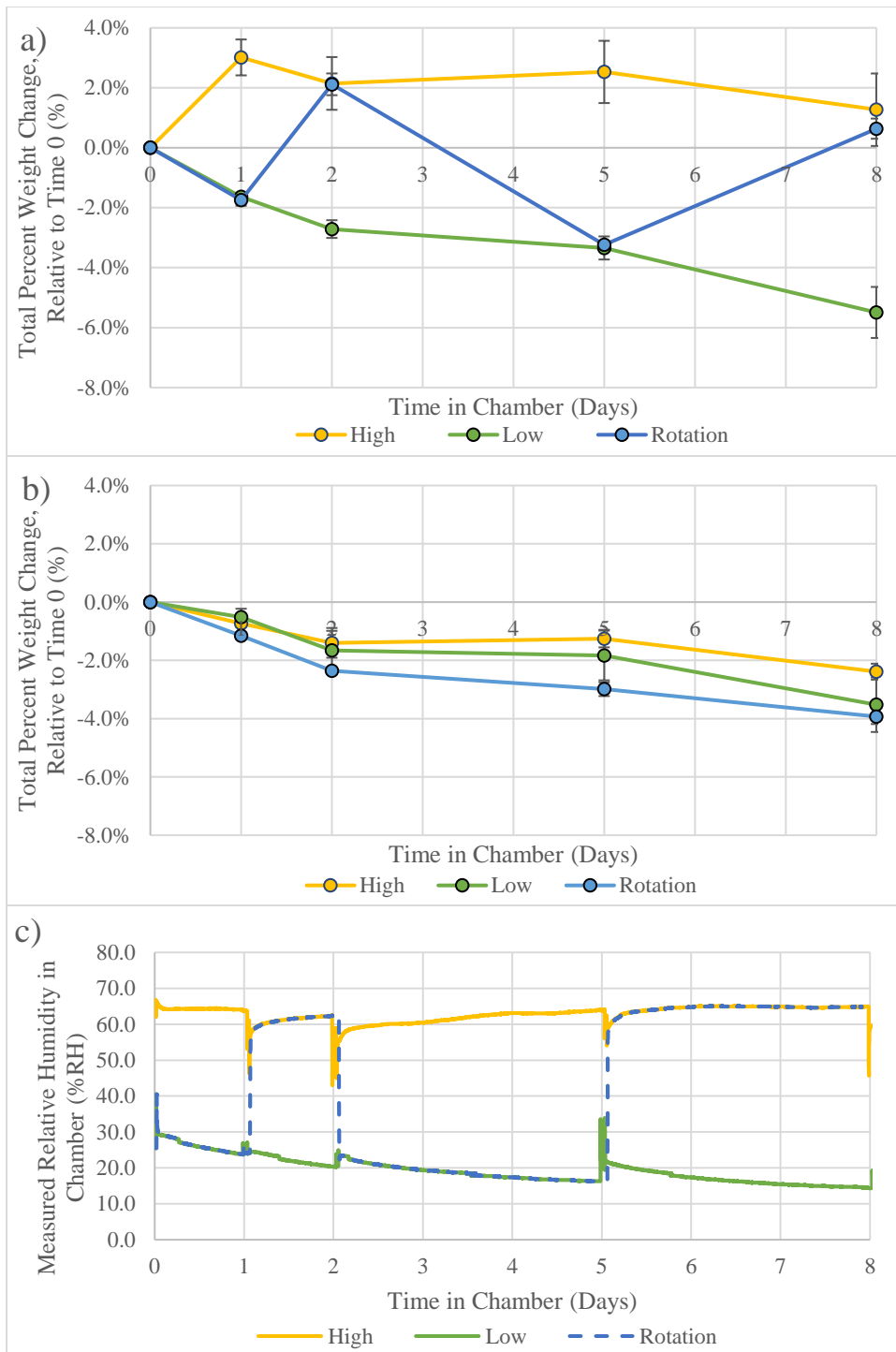


Figure 4.3 Change in bulk weight of a) maltodextrin-based or b) erythritol-based DNATrax material in response to c) the relative humidity in each chamber. Error bars indicate the standard deviations of triplicate samples. Numerical values for bulk weights can be found in Tables 4A.1 and 4A.2.

The bulk weight of maltodextrin material rotated between the low- and high-humidity chambers decreased and increased according to the chamber in which it was stored (Figure 4.3a). Moisture was removed from the material after each incubation at low humidity, with decreases in weight from the starting value of $1.7\pm 0.2\%$ and $3.2\pm 0.1\%$ on days 1 and 5, respectively, relative to the starting weight. There was no significant difference between the weight change in the rotated material and those stored consistently in the low humidity chamber, even on day 5 when the rotated samples lost 2.1% of their weight more in water over 2 fewer days of incubation. The consistency between the low humidity samples and the rotated samples on day 5 supports the conclusion that the gradual decrease in weight of the low humidity material is due to the gradual decrease in chamber humidity. Similarly, when rotated samples were placed in the high humidity chamber, they reached the same equilibrium weight change at days 2 and 8 ($2.1\pm 0.4\%$ and $0.6\pm 0.3\%$, respectively) as those consistently stored in the high humidity chamber ($2.1\pm 0.9\%$ and $1.3\pm 1.2\%$, respectively). This consistency of the rotated maltodextrin material with its single-chamber counterparts indicates the reversibility of the water absorption/desorption process in maltodextrin.

For particle transport purposes, it is not the bulk weight of the material, but the effect of changes in the material density and the corresponding aerodynamic diameter that is of concern. Changes in weights of maltodextrin particles ranged from -5.5% (low humidity incubation for 8 days) to +3.0% (high humidity incubation for 1 day). An 8.5% increase in weight with no change in physical diameter, as might be expected if moisture was absorbed into pores, would increase the density by 8.5%. Since the aerodynamic diameter of a particle is proportional to the square root of the particle's density (Equation 4.3), this would result in a 4.16% change in aerodynamic diameter. Thus, a maltodextrin particle with a 2.00- μm aerodynamic diameter at low humidity

would have an aerodynamic diameter of 2.08 μm at high humidity. This change is small compared to the variability between replicate aerodynamic diameter measurements of the same aliquot, which can be as high as 10%. Thus, the change in aerodynamic diameter due to the absorption of moisture by the maltodextrin material is negligible.

While maltodextrin's hygroscopic nature was revealed in the high and low humidity chambers, incubation of erythritol material confirmed its nonhygroscopic nature at these humidities (Figure 4.3b). The weight of the erythritol material decreased between 0.2% and 1.7% at each time point, regardless of which humidity condition was used for storage. Additionally, there was no significant difference in weight between the two storage conditions occurring until after 8 days of storage. Given that the high humidity chamber reached a maximum relative humidity of 66.7%, this result is consistent with previous reports that erythritol does not readily absorb moisture at relative humidities below 90%¹⁰. However, the gradual decrease in weight over time suggests that the material had residual moisture present at the start that was desorbed over time. Since the material was stored in a sealed vial in a desiccator between production and the start of the experiment, the desorbed moisture is likely residual moisture from the spray-drying production process. In future hygroscopicity studies, it would be beneficial to dry material to a constant weight under defined relative humidity before making the initial weight measurements.

4.3.3 Effect of Humidity Exposure on Particle Size

While neither material exhibited enough water absorption to significantly change the material's density and corresponding aerodynamic diameter, the aerodynamic diameter can also be altered through particle agglomeration. Particle agglomeration will form larger, irregularly

shaped clusters with higher aerodynamic diameters. To determine if this agglomeration significantly affected either material, the aerodynamic diameters of particles in each material were also assessed at each time point.

As the bulk weight changes suggested, the MMAD and d90 aerodynamic diameters for both maltodextrin (Figure 4.4) and erythritol (Figure 4.5) showed no significant difference between material stored at either high and low humidity until after 8 days of incubation (95% confidence). Additionally, the MMADs and d90s of the rotated aliquots were indistinguishable from the high- and low-humidity aliquots with few exceptions. The d90 of the rotated maltodextrin was significantly lower than that of both the high and low humidity samples on day 1, and both the MMAD and d90 were significantly higher than those for the low humidity samples on day 8 (95% confidence). For erythritol, the d90 of the rotated material was significantly lower than that of the high humidity samples on day 1 and significantly higher than that of the low humidity samples on day 2 (95% confidence).

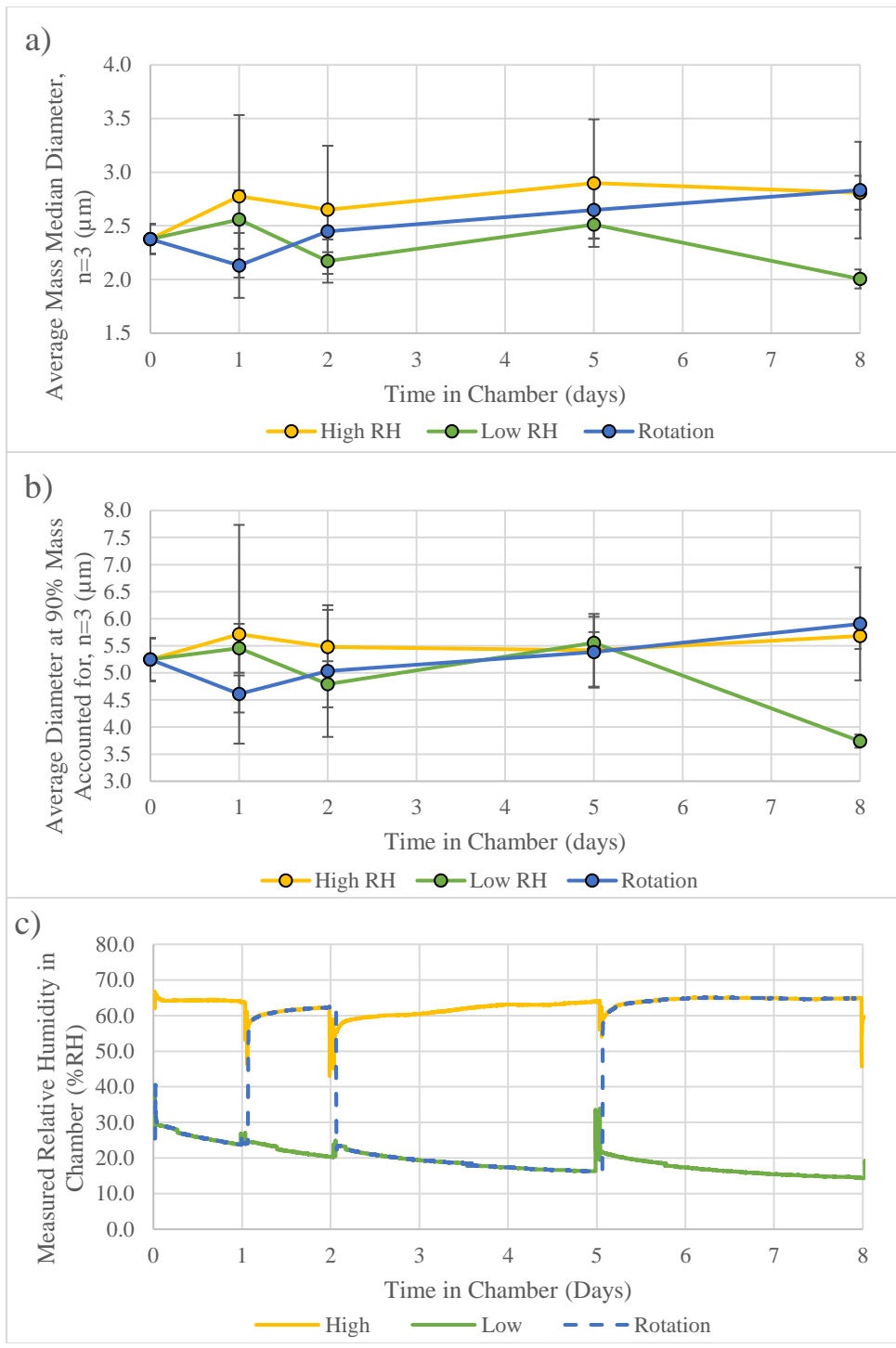


Figure 4.4 Average aerodynamic diameter of maltodextrin-based particles assessed using a) the MMAD and b) the d90 after incubation at high humidity, low humidity, or both on a rotating basis according to the c) humidity profiles. Error bars indicate the standard deviation of triplicate samples. Numerical values for bulk weights can be found in Tables 4A.3 and 4A.4.

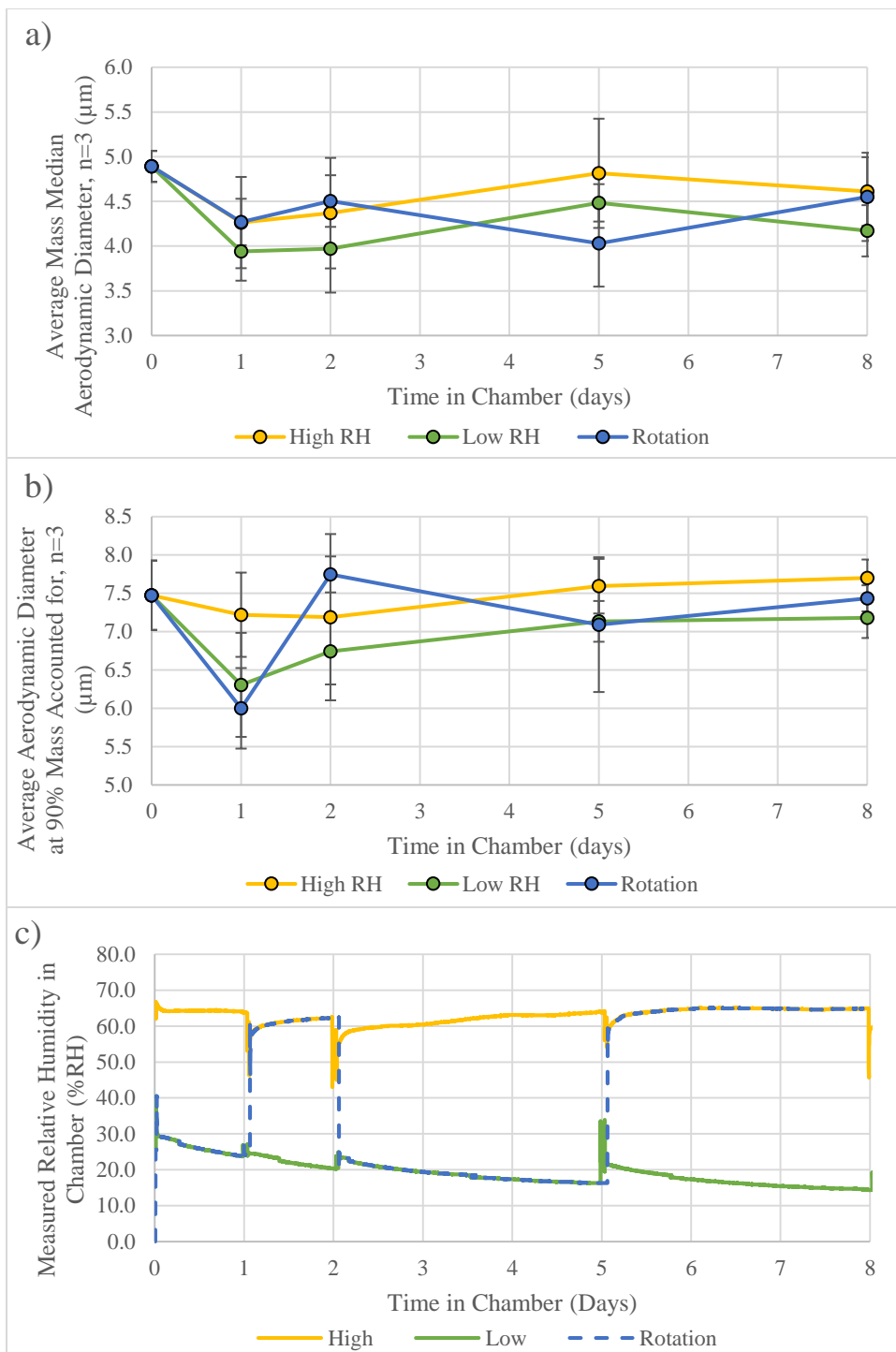


Figure 4.5 Average aerodynamic diameter of erythritol-based particles assessed using a) the MMAD and b) the d_{90} after incubation at high humidity, low humidity, or both on a rotating basis according to the c) humidity profiles. Error bars indicate the standard deviation of triplicate samples. Numerical values for bulk weights can be found in Tables 4A.5 and 4A.6.

The lack of size changes indicates that significant, irreversible agglomeration of particles did not occur during sample storage and the aerodynamic diameters of maltodextrin and erythritol particles were stable at both humidities tested. Any particles agglomerates formed were weakly held together and broken apart by the eductor during aerosolization, resulting in no net change in the aerodynamic diameter. The lack of a significant change in particle size across this range of humidities (14.4% to 64.9%) is a positive characteristic for material to be used in field tests, where humidity can be monitored but not controlled. However, while there was minimal size change across this range, the humidity levels were kept below the critical relative humidity. At humidities above the critical value, the material will rapidly increase in moisture content with a slight increase in humidity. Since the extent of moisture absorbance affects aerodynamic diameter not only by increasing the density of the material but also through facilitating particle agglomeration, the results here cannot be extended to humidities above the critical relative humidity. Additional tests are needed to draw conclusions about particle size stability under those conditions.

4.3.4 Effect of Humidity Exposure on DNA Degradation

Unlike the particle size, which experienced no significant change during incubation in the humidity chambers, a significant decrease in the amount of DNA quantified using qPCR was measured for both maltodextrin and erythritol DNA Trax material after 8 days of chamber incubation as well when stored at ambient conditions (Figure 4.6). In all cases, light exposure was restricted to ambient light in the lab during weight measurements and processing for PCR. Both the DNA-labeled maltodextrin and erythritol materials started with similar levels of

labeling (670 copies of DNA per particle of 2- μ m diameter) and DNA labeling decreased significantly with the 8-day incubation in all storage conditions (95% confidence).

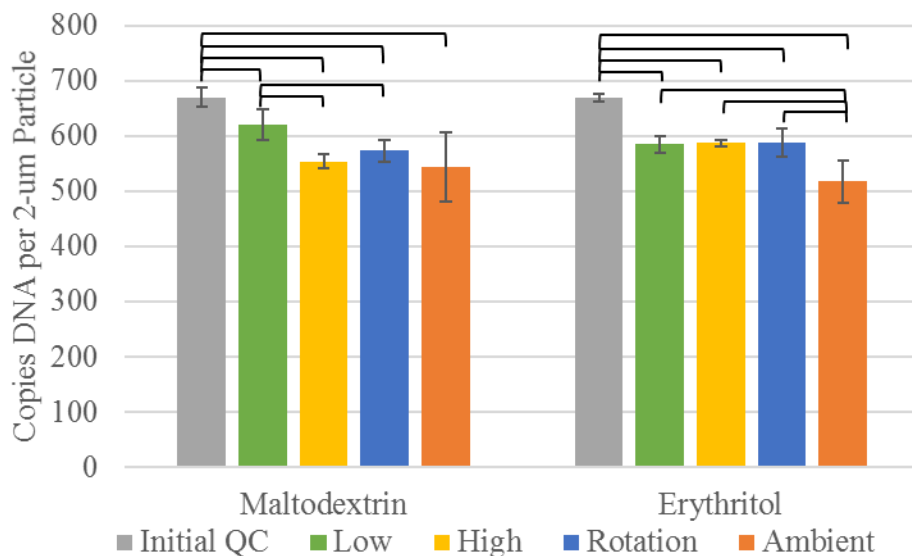


Figure 4.6 Copies of replicable DNA per particle with a 2- μ m aerodynamic diameter in maltodextrin-based and erythritol-based DNATrax material as determined by qPCR after storage at low humidity, high humidity, rotation between low and high humidity, or ambient conditions. Error bars are the standard deviation of 3 samples. Significant differences between DNA levels are indicated by the brackets (95% confidence).

In the erythritol material, the three sets of aliquots stored within closed chambers (low, high, and rotation aliquots) degraded in a similar manner with 584 ± 14 , 587 ± 6 , and 587 ± 26 copies/particle (respectively) remaining after storage (Table 4A.8). Given that erythritol is nonhygroscopic at the humidity levels in either chamber and did not absorb moisture during the time of incubation, it can be concluded that the primary mechanism in DNA degradation in the erythritol material is independent of humidity level or the presence of water in the material. One

possible mechanism of this degradation is through hydrolytic cleavage of the DNA backbone by DNases present in the material. Some precautions were taken to limit the contamination of DNases in the DNATrax material during material production and storage including bleaching glassware before use, using PCR-grade (DNase- and RNase-free) water, and autoclaving storage vials. However, the drying gas used for production was heated ambient air that was not filtered prior to use. Thus, airborne contaminants could be incorporated into the material during particle generation. The likelihood of DNase activity contributing to the degradation of DNA is also supported by the erythritol ambient samples undergoing significantly more degradation than those in closed humidity chambers with only 543 copies/particle remaining. While the low, high, and rotation aliquots were placed in sealed chambers, the ambient samples were placed uncapped on the benchtop and would be more susceptible to contamination by microbial DNases. Although DNase contamination and the subsequent DNA degradation is independent of humidity and would be more likely to occur for material open to room air rather than in a closed chamber, further experiments are required to test this hypothesis.

The results for the DNA stability in the maltodextrin material are not as clear. While the ambient samples did experience the greatest decrease in DNA after incubation (543 copies/particle; 81.1% remaining), this decrease was not significantly more than storage in the humidity chambers. Additionally, the samples stored in the low humidity chamber underwent less degradation than those in the high chamber or rotated between chambers. Maltodextrin did absorb moisture at high humidity and, while this did not significantly alter the particle size, it does appear to play a role in the extent of DNA degradation. At all times, the ambient samples were at relative humidities between those of the high and low humidity chambers (Figure 4.7), so if the primary mechanism of degradation depended solely on the presence of humidity, then the

ambient aliquots would have DNA labeling between those of the high and low chambers. Since this is not the case, there are likely multiple degradation mechanisms occurring and the DNase activity suspected in the erythritol material also plays a role in DNA degradation in the maltodextrin material.

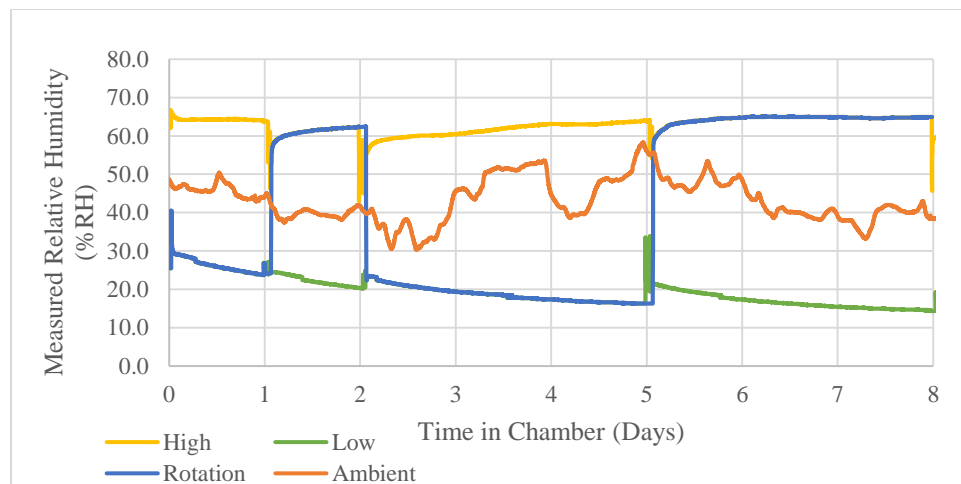


Figure 4.7 Relative humidity experienced by aliquots stored in high- or low-humidity chambers, rotated between them, or stored on the benchtop under ambient condition.

4.4 Conclusions

While fluctuations in humidity are likely during aerosol transport tests in outdoor environments, the stability of the aerodynamic diameter and persistence of the DNA label in DNATrax material were not significantly affected by this variable. Two sweeteners, maltodextrin and erythritol, both produced free-flowing powders and were both determined to be suitable for bulk material production. While maltodextrin exhibited some (<10%) absorption of moisture, this did not result in a significant increase in the aerodynamic diameter through either particle swelling or agglomeration. Production yields of erythritol were an order of magnitude

lower than maltodextrin, but no moisture was absorbed during incubation at high relative humidity (63% RH). While the amount of amplifiable DNA decreased between 7 and 18% after 8 days of storage, there was no correlation between the extent of degradation and the humidity used, indicating the DNA label is not significantly affected by the presence or lack of humidity at these values. Further work is required to confirm the stability of the material at humidities above the critical relative humidity of each material. Overall, DNATrax material made from either maltodextrin or erythritol is stable over a range of humidities (up to 65% RH) and can be used in environments where the humidity is variable.

APPENDIX

APPENDIX

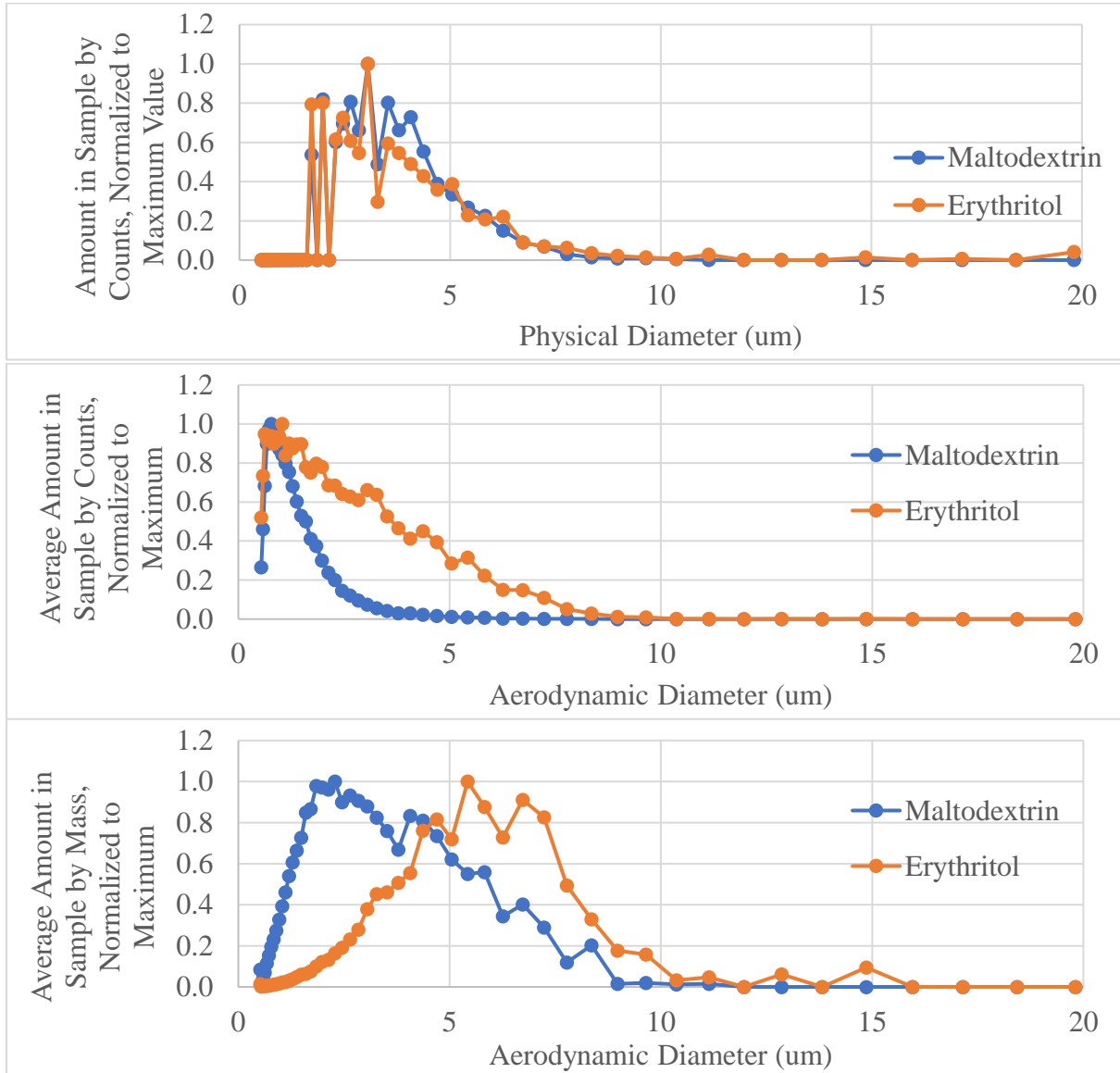


Figure 4A.1 Particle size distributions for maltodextrin and erythritol-based DNATrax plotted as the a) physical diameter scaled by counts, b) aerodynamic diameter scaled by counts, and c) aerodynamic diameter scaled by mass.

Maltodextrin	Metric	Day 0	Day 1	Day 2	Day 5	Day 8
Low	Average	0.00%	-1.64%	-2.71%	-3.34%	-5.49%
	St. Dev.	0.00%	0.08%	0.30%	0.39%	0.85%
High	Average	0.00%	3.01%	2.15%	2.53%	1.27%
	St. Dev.	0.00%	0.60%	0.88%	1.04%	1.21%
Rotation	Average	0.00%	-1.75%	2.12%	-3.24%	0.64%
	St. Dev.	0.00%	0.19%	0.36%	0.09%	0.34%

Table 4A.1 Changes in bulk weight relative to the starting weight for maltodextrin material.

Averages and standard deviations are for n=3 aliquots.

Erythritol	Metric	Day 0	Day 1	Day 2	Day 5	Day 8
Low	Average	0.00%	-0.51%	-1.66%	-1.83%	-3.52%
	St. Dev.	0.00%	0.28%	0.67%	0.85%	0.94%
High	Average	0.00%	-0.73%	-1.40%	-1.25%	-2.39%
	St. Dev.	0.00%	0.12%	0.51%	0.30%	0.27%
Rotation	Average	0.00%	-1.16%	-2.36%	-2.99%	-3.93%
	St. Dev.	0.00%	0.03%	0.04%	0.24%	0.26%

Table 4A.2 Changes in bulk weight relative to the starting weight for erythritol material.

Averages and standard deviations are for n=3 aliquots.

Maltodextrin, MMAD	Metric	Day 0	Day 1	Day 2	Day 5	Day 8
Low	Average	2.38	2.56	2.17	2.51	2.01
	St. Dev.	0.14	0.27	0.20	0.13	0.09
High	Average	2.38	2.78	2.65	2.90	2.81
	St. Dev.	0.14	0.76	0.60	0.59	0.16
Rotation	Average	2.38	2.13	2.45	2.65	2.83
	St. Dev.	0.14	0.30	0.19	0.27	0.45

Table 4A.3 Average MMAD values for maltodextrin material. Averages and standard deviations are for n=3 aliquots.

Maltodextrin, d90	Metric	Day 0	Day 1	Day 2	Day 5	Day 8
Low	Average	5.25	5.46	4.79	5.56	3.74
	St. Dev.	0.40	0.45	0.43	0.20	0.12
High	Average	5.25	5.71	5.48	5.42	5.68
	St. Dev.	5.25	2.02	0.69	0.67	0.24
Rotation	Average	0.40	4.61	5.04	5.38	5.90
	St. Dev.	5.25	0.34	1.22	0.66	1.04

Table 4A.4 Average d90 values for maltodextrin material. Averages and standard deviations are for n=3 aliquots.

Erythritol, MMAD	Metric	Day 0	Day 1	Day 2	Day 5	Day 8
Low	Average	4.89	3.94	3.97	4.48	4.17
	St. Dev.	0.17	0.33	0.49	0.21	0.29
High	Average	4.89	4.26	4.37	4.81	4.61
	St. Dev.	0.17	0.51	0.62	0.61	0.38
Rotation	Average	4.89	4.27	4.50	4.03	4.55
	St. Dev.	0.17	0.26	0.29	0.48	0.49

Table 4A.5 Average MMAD values for erythritol material. Averages and standard deviations are for n=3 aliquots.

Erythritol, d90	Metric	Day 0	Day 1	Day 2	Day 5	Day 8
Low	Average	7.47	6.31	6.74	7.13	7.18
	St. Dev.	0.45	0.68	0.43	0.27	0.26
High	Average	7.47	7.22	7.19	7.59	7.70
	St. Dev.	0.45	0.55	1.09	0.36	0.24
Rotation	Average	7.47	6.00	7.75	7.09	7.44
	St. Dev.	0.45	0.53	0.24	0.88	0.17

Table 4A.6 Average d90 values for erythritol material. Averages and standard deviations are for n=3 aliquots.

Maltodextrin	Initial QC	Low	High	Rotation	Ambient
Average	670	620	553	574	543
Standard Deviation	16	28	13	20	64
% Intact DNA	100.0%	92.5%	82.6%	85.6%	81.1%

Table 4A.7 Copies of DNA per 2- μ m particle of maltodextrin-based DNATrax as determined using qPCR. Averages and standard deviations are for n=3 aliquots.

Erythritol	Initial QC	Low	High	Rotation	Ambient
Average	669	584	587	587	517
Standard Deviation	8	14	6	26	37
% Intact DNA	100.0%	87.3%	87.8%	87.7%	77.3%

Table 4A.8 Copies of DNA per 2- μ m particle of erythritol-based DNATrax as determined using qPCR. Averages and standard deviations are for n=3 aliquots.

REFERENCES

REFERENCES

1. Weather Underground. www.wunderground.com. The Weather Channel Interactive, Inc. Atlanta, GA. Last accessed June 12, 2017.
2. Juarez-Enriquez E, Olivas GI, Zamudio-Flores PB, Ortega-Rivas E, Perez-Vega S, Sepulveda DR. Effect of water content on the flowability of hygroscopic powders. *J Food Eng.* 2017. 205: 12-17.
3. Radosta S, Schierbaum F, Reuther F, Ager H. Polymer-water interaction of maltodextrins. Part I. Water vapour sorption and desorption of maltodextrin powders. *Starch/Stärke.* 1989. 41: 395-401.
4. Ávila EL, Rodríguez MC, Velásquez HJC. Influence of maltodextrin and spray drying process conditions on sugarcane juice powder quality. *Rev Fac Nac Agron.* 2015. 68: 7509-7520.
5. Goula AM, Adamopoulos KG. Effect of maltodextrin addition during spray drying of tomato pulp in dehumidified air: II. powder properties. *Dry Technol.* 2008. 26: 726-737.
6. Caparino OA, Tang J, Nindo CI, Sablani SS, Powers JR, Fellman JK. Effect of drying methods on the physical properties and microstructures of mango (Philippine 'Carabao' var.) powder. *J Food Eng.* 2012. 111: 135-148.
7. Harding RN, Hara CA, Hall SB, Vitalis EA, Thomas CB, Jones AD, Day JA, Tur-Rojas VR, Jorgensen T, Herchert E, Yoder R, Wheeler EK, Farquar GR. Unique DNA-barcoded aerosol test particles for studying aerosol transport. *Aerosol Sci Technol.* 2016. 50: 429-435.
8. Perko R and DeCock P. Erythritol. In: *Sweeteners and Sugar Alternatives in Food Technology.* H Mitchell, ed. Blackwell Publishing: Oxford, UK. 2006. 151-176
9. Avaltroni F, Bouquerand PE, Normand V. Maltodextrin molecular weight distribution influence on the glass transition temperature and viscosity in aqueous solutions. *Carbohydr Polym.* 2004. 58: 323-334.
10. DeCock P. Erythritol. In: *Alternative Sweeteners, 4th Ed.* LOB Nabors, ed. CRC Press, Taylor & Francis Group: Boca Raton, FL. 2012. 249-264.
11. Bhandari BR, Adhikari BP. Water activity in food processing and preservation. In: *Drying Technologies in Food Processing, 1st Ed.* XD Chen, AS Mujumdar, eds. Blackwell Publishing: Oxford, UK. 2008. 55-89.
12. Hyvönen L, Koivistoninen P. Food technological evaluation of xylitol. *Adv Food Res.* 1983. 373-403.

13. Sträter PJ. Palatinit - Technological and processing characteristics. In: *Alternative Sweeteners*. LOB Nabors, RC Gelardi, eds. Marcel Dekker: New York. 1986. 217-244.
14. Morris CE. New applications for maltodextrin. *Food Eng.* 1984. 56: 48-50.
15. Castro N, Durrieu V, Raynaud C, Rouilly A. Influence of DE-value on the physicochemical properties of maltodextrin for melt extrusion processes. *Carbohydr Polym.* 2016. 144: 464–473.
16. Hinds WC. *Aerosol Technology: Properties, Behavior, and Measurement of Airborne Particles*, 2nd Ed. John Wiley and Sons, Inc.: New York, NY. 1999.
17. Mitchell JP, Nagel MW. Time-of-flight aerodynamic particle size analyzers: their use and limitations for the evaluation of medical aerosols. *J Aerosol Med.* 1999. 12: 217-240.
18. TSI. Aerodynamic Particle Sizer Model 3321: Theory of Operation. 2012. www.tsi.com.
19. Lund S, Dissing J. Surprising stability of DNA in stains at extreme humidity and temperature. *Int Congr Ser.* 2004. 1261: 616–618.
20. Mouret S, Philippe C, Gracia-Chantegrel J, Banyasz A, Karpati S, Markovitsi D, Douki T. UVA-induced cyclobutane pyrimidine dimers in DNA: a direct photochemical mechanism? *Org Biomol Chem.* 2010. 8: 1706–1711.
21. Udey, RN. Statistical data analyses of trace chemical, biochemical, and physical analytical signatures. *Doctoral dissertation*. 2013. Retrieved from MSU Libraries.
22. Wexler A, Hasegawa S. Relative humidity-temperature relationships of some saturated salt solutions in the temperature range 0 to 50 C. *J Res Nat Bur Stand.* 1954. 53: 19-26.
23. Roos YH. Water activity and physical state effects on amorphous food stability. *J Food Process Pres.* 1993. 16: 433–447.

CHAPTER FIVE: Conclusions

From individual barcode quantification during multiplexed experiments to environmental stability for outdoor studies, the advantages posited at the inception of DNATrax have been largely proved true. When coupled with passive sampling, this aerosol tracer can provide high-resolution spatial distributions of particle deposition across a defined space. Unlike the detection scheme in many other tracers, the DNA signature used here is tunable, allowing for experiment multiplexing and reproducibility assessments during field tests, a rarity among aerosol transport studies. The particle size and DNA label are stable at relative humidities up to 66%, as well as in varying humidities in that range, and the solid particle affords the DNA label some protection when exposed to UV radiation. However, there remain additional aspects of field studies that should be considered before its use.

For indoor studies, the combination of passive sampling with the DNA tagged particles is a powerful combination for high-resolution sampling. However, the passive sampling material selected for an experiment should be checked for compatibility with the qPCR assay before each use, as some commercial products such as Post-It® notes vary in qPCR compatibility between packs.

Outdoor studies present additional variables to consider. The DNA tag was found to degrade with exposure to UV radiation, although the solid material offered some protection. However, it should be noted that the UV exposure here is an imperfect model of the wavelengths and relative intensities within sunlight and additional work should be done using actual sunlight. While shown to be stable under variable humidities up to 66%, the DNA tag did experience some degradation over a week of storage in uncapped vials. When not kept under sterile

conditions, contamination by DNases in the environment will lead to DNA degradation. Contamination by DNases becomes even more prevalent in outdoor studies and could cause significant degradation in material during experiments lasting 1 week or longer. This would have to be taken into account when evaluating results from such studies. An additional consideration for longer studies is the variation in humidity that can occur. While neither maltodextrin or erythritol bulk materials were negatively affected by humidities as high as 66%, increased moisture absorption at humidity levels above their critical relative humidity values could lead to altered particle transport and agglomeration. Additionally, dew formation or precipitation occurring during the course of a longer study would be detrimental to the DNATrax material, as the particles are water-soluble. While the DNA tag could still be collected from the aqueous samples after dissolution, the DNA tag is more susceptible to UV photodegradation in its aqueous form. For long-term outdoor studies where precipitation is likely to occur, alternative materials should be investigated for production of particles that are not water soluble and would maintain the protection of the DNA tag for the duration of such experiments.

The ability to perform simultaneous aerosol transport experiments is a novel aspect of this work and the power of this experimental design is fully realized when it is coupled with computational models. The validation of models using experimental data is vital to their accurate prediction of particle transport in complex spaces. An experimental design that allows particle deposition pattern to be determined from a variety of release and sampling locations, each under identical environmental conditions, provides a simple platform for acquiring the necessary data for model validation, with DNATrax already being used for this purpose by other research scientists and government agencies.